IEEE Access
Multidisciplinary ⋮ Rapid Review ⋮ Open Access Journal

Received 27 August 2024, accepted 15 September 2024, date of publication 19 September 2024, date of current version 7 October 2024.

*Digital Object Identifier 10.1109/ACCESS.2024.3464231*

RESEARCH ARTICLE

# Resource-Efficient Derivative PPG-Based Signal Quality Assessment Using One-Dimensional CNN With Optimal Hyperparameters for Quality-Aware PPG Analysis

**YALAGALA SIVANJANEYULU[1], M. SABARIMALAI MANIKANDAN[2], (Senior Member, IEEE), SRINIVAS BOPPU[1], (Member, IEEE), AND LINGA REDDY CENKERAMADDI[3], (Senior Member, IEEE)**

[1]School of Electrical Sciences, Indian Institute of Technology Bhubaneswar, Bhubaneswar 752050, India
[2]Department of Electrical Engineering, Indian Institute of Technology Palakkad, Palakkad 678623, India
[3]Department of ICT, University of Agder, 4898 Grimstad, Norway

Corresponding author: Linga Reddy Cenkeramaddi (linga.cenkeramaddi@uia.no)

This work was supported in part by the Indo-Norwegian Collaboration in Autonomous Cyber-Physical Systems (INCAPS) under Project 287918 and in part by the International Partnerships for Excellent Education, Research and Innovation (INTPART) Program from the Research Council of Norway.

**ABSTRACT** Photoplethysmogram (PPG) is a bio-optical technology used heavily in wearable health devices for monitoring vital sign parameters. Therefore, ensuring the quality of PPG signals is crucial for accurate measurements, as these signals are susceptible to various artifacts and noises. This article proposes a derivative-based PPG (dPPG) signal quality assessment (SQA) method to distinguish high-quality data from artifact-laden signals. The proposed method includes a first-order derivative, followed by a 3-point moving average filter to smooth the high-frequency components present in the dPPG signal. Further, the smoothed dPPG signal is fed into 2, 4, and 6-layer 1D-convolutional neural networks (1D-CNN) to classify it as a clean or noisy dPPG signal. The proposed derivative-based PPG-SQA method is tested using various PPG signals collected from standard databases. The noisy PPG signals are collected from the wrist-cup (WC-PPG) database, whereas acceleration (SYN-ACCE-PPG) and random noise (SYN-RN-PPG) affected PPG signals are synthetically generated using noise-free PPG (NF-PPG) signals. We evaluate the proposed method using performance metrics like sensitivity (SE), specificity (SP), accuracy (ACC), model size (in MB), and processing time (PT). We also implemented the proposed method on the Raspberry Pi 4 (R-Pi-4) to study its real-time feasibility. The 6-layer 1D-CNN with 32 kernels using the ReLU activation function is observed to outperform the other models and existing PPG-SQA methods. The proposed method, when compared to NF signals, achieves: 99.84% of SE, 97.94% of SP, and 99.70% of ACC for WC-PPG; 99.79% of SE, 100.00% of SP, and 99.96% of ACC for SYN-RN-PPG; and 84.48% of SE, 74.63% of SP, and 78.17% of ACC for SYN-ACCE-PPG, respectively. Results demonstrate that selecting the appropriate 1D-CNN model can achieve higher SE, SP, and ACC with a lower computational load on PC-CPU and R-Pi computing platforms. Furthermore, we test the reliability and robustness of the dPPG-1D-CNN-SQA model using the unseen databases. Our model may reduce the false alarms and energy consumption of wearable healthcare devices, which have limited battery capacity and computational resources.

**INDEX TERMS** PPG signal quality assessment, PPG signal analysis systems, blood pressure estimation, PPG-derived respiration rate, false alarm reduction, wearable health monitoring devices, convolutional neural network.

The associate editor coordinating the review of this manuscript and approving it for publication was Ines Domingues.

## I. INTRODUCTION

Photoplethysmogram (PPG) is a bio-optical technology used to detect changes in blood volume or blood flow rate in the

© 2024 The Authors. This work is licensed under a Creative Commons Attribution-NonCommercial-NoDerivatives 4.0 License.
For more information, see https://creativecommons.org/licenses/by-nc-nd/4.0/

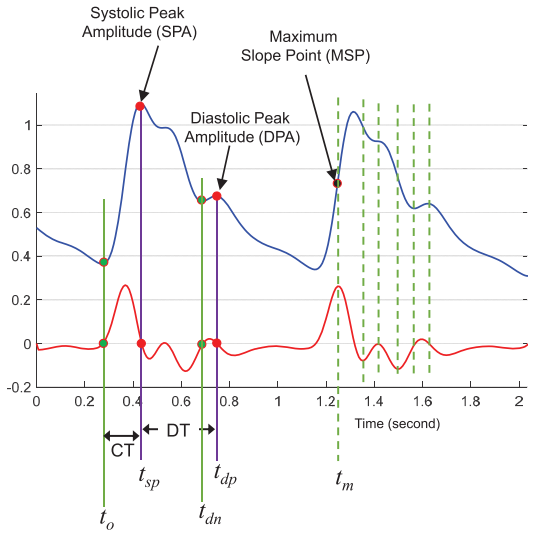


**FIGURE 1.** (a) Original PPG signal (blue) and the first derivative of PPG (red) with positive zero-crossing points (green) and negative zero-crossing points (red).

microvascular bed of tissues. PPG is a relatively simple, non-invasive, convenient, and cost-effective technology widely used in various Internet of Things (IoT) enabled wearable and portable health monitoring devices (e.g., smart watches, smart rings, smartphones) and remote health monitoring devices [1], [2], [3]. These PPG-embedded wearable and portable devices enable the continuous monitoring of vital sign parameters such as pulse rate [4], blood oxygen saturation rate ($SPO_2$) [5], [6], respiration rate [4], [7], [8], blood pressure [9], [10], [11], and blood glucose level [12]. However, the PPG signals are highly susceptible to noises and artifacts during acquisition [13]. These noises and artifacts are categorized into four types: *baseline drift*, *motion artifact*, *electrical interference*, and *sensor disconnection* [14], [15], [16]. However, the PPG signal is mainly contaminated with motion/movement artifacts due to sensor movement and physical activity, and its frequency range is greater than 0.1 Hz [17]. Removing the motion artifacts from the PPG signal is the most challenging task due to its overlapping frequency range with the desired signal range.

### A. SIGNIFICANCE OF DERIVATIVE-BASED PPG QUALITY ASSESSMENT

Fig. 1 shows a raw and its first-order derivative PPG signals. The first-order derivative PPG signal's zero-crossing points (positive and negative) and maximum peak represent the location of fiducial points (onset, peak, and maximum slope point) in the raw PPG signal; see Fig. 1. In most PPG analysis applications, derivatives of PPG are used for the following purposes [14], [16], [18]:

- Extracting PPG parameters and clinical indexes such as systolic peak [19], systolic onset [19], [20], systolic slope [21], midpoint, crest time, decay time, pulse width, pulse area, augmentation index, atrial stiffness index [22], and reflection index associated with cardiovascular diseases [23], [24], [25].
- Extracting PPG waveform features for automatically estimating beat-to-beat blood pressure [26], [27], [28], [29].
- Measuring respiration rate from respiratory induced PPG variations such as amplitude variation (amplitude modulation), baseline variation (baseline modulation), peak to peak interval (PPI) variation (frequency modulation) [15], [30], [31].
- PPG cycle extraction (previous onset to next onset) for PPG waveform morphology-based cardiac arrhythmia recognition and bio-metric authentication [32] in addition to measurement of vital signs directly from PPG signals, including $SPO_2$ [6], [33], pulse rate [34], beat-to-beat intervals, and blood glucose level [35].

The deflection points of the derivative signals provide valuable information about clinical parameters. Fiducial points such as onset [36], systolic peak [36], slope, midpoint, tidal wave peak, dictotic notch, and diastolic wave peak, which can be distorted even in the presence of low-level noises or artifacts, can be emphasized in the derivative signal. Fig. 2 shows the normal and abnormal PPG signals, motion artifacts (MA) corrupted PPG signal, random-noise corrupted PPG signals and their first, second, and third derivatives of the PPG signal [18], [37], [38], [39]. Due to unavoidable noisy PPG signals under ambulatory and exercise recording scenarios using wearable and portable sensing devices, an automatic signal quality assessment (SQA) of PPG has become essential for ensuring accurate and reliable health monitoring with reduced false alarms [16], [40], [41]. The high-frequency components of noises and artifacts are emphasized with increasing the order of the derivatives, as shown in Fig. 2. The deflection points of the PPG signal are most essential for the measurement of PPG parameters and clinical indexes, but fiducial points are completely masked and distorted in derivatives of the PPG signal when corrupted with noises and artifacts, as shown in Fig. 2. Therefore, in this study, we have proposed the first-order derivative PPG signal as the input to the one-dimensional convolutional neural network (1D-CNN) for assessment of the quality of PPG signals.

By detecting the presence of noise and artifacts before performing automatic PPG analysis, we can improve the accuracy and trustworthiness of health monitoring devices and PPG-based biometric and emotional state recognition systems [15], [32], [42]. In this paper, by considering the resource constraints of affordable wearable or portable health monitoring devices and long-term continuous monitoring scenarios, we present a derivative PPG-based 1D-CNN signal quality assessment method to classify the PPG signals into clean or noisy by finding the best activation function and optimal hyperparameters with a major objective of detecting noisy PPG signals having different patterns of normal and abnormal PPG signals and levels of noises and artifacts. The quality-aware PPG analysis system leads to not only

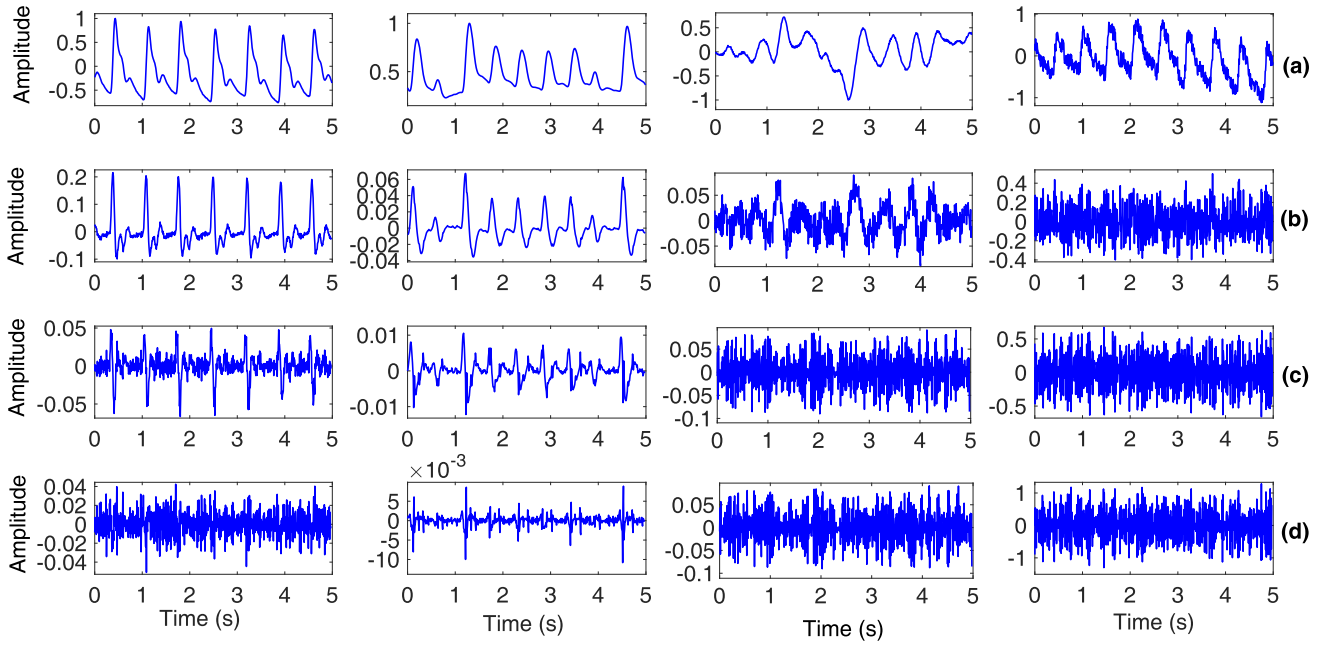


**FIGURE 2.** (a) From left to right: 5-second noise-free, abnormal, motion artifact, random noise added PPG segments, which are taken from MIT-BIH Polysomnographic database (record name: SLP02a), UCI database (subject number: 9003), wrist database (record name: $s2_{walk}$), and BIDMC database (record name: bidmc40), respectively. (b), (c), and (d) show the corresponding first, second, and third derivatives of original PPG segments shown in (a), respectively.

better disease diagnosis and prediction outcomes, but it can also improves the energy efficiency of continuous PPG-based health and wellness monitoring devices with the salient feature of discarding noisy PPG signals from further processing, compression [43], [44], transmission, and storage [45], [46].

### B. MAJOR CONTRIBUTIONS AND ORGANIZATION OF THIS ARTICLE

In this article, we explore the dPPG-based 1D-CNN-SQA method with 2, 4, and 6 convolutional layers with three distinct activation functions such as ReLU, LeakyReLU, and Tanh. We have also considered 16, 32, and 64 kernels with a kernel size of 3. To achieve the efficient dPPG-SQA method, the CNN models were evaluated using various standard and in-house databases collected from multiple devices. The main contributions of this paper are summarized below:

- Finding the best activation function and optimal hyper-parameters of 1D-CNN to achieve higher accuracy, sensitivity, and specificity with reduced latency, computation complexity, and model size under different kinds of noise-free normal, abnormal PPG signals, movement artifacts corrupted PPG signals, and random noises corrupted PPG signals with different noise levels.
- Demonstrate real-time feasibility of the best CNN-based PPG signal quality assessment method on R-Pi computing platform and its performance comparison with a high-performance computer. The R-Pi-4 model B includes the Quad-Core Cortex-A72 processor, 8 GB LPDDR4 RAM, and 32 GB ROM.
- Unlike other existing SQA methods, the performance of the CNN model is evaluated using a wide variety of normal and abnormal PPG signals taken from untrained PPG databases, which are used in the studies for performance evaluations of blood pressure estimation methods, respiration rate estimation methods, sleep apnea detection methods, pulse rate estimation methods, and cardiac arrhythmia recognition methods.
- Performance of the 1D-CNN-based PPG SQA method and dPPG-based 1D-CNN-SQA method is compared in addition to performance comparison with other existing methods in terms of sensitivity, specificity, overall accuracy, latency, and model size.

The rest of this article is structured in the following manner: Section II presents the related work. Section III presents the 2, 4, and 6 layer 1D-CNN-based dPPG-SQA method. Details of the database and implementation are given in Section IV. Section V presents the evaluation results of the dPPG-SQA method for the different number of layers, activation functions, and kernels. Conclusions are presented in Section VI.

## II. RELATED WORK

In this section, we summarize both conventional (non-DL-based) and DL-based PPG SQA methods from the literature and differentiate our work from them.

### A. FEATURES BASED PPG SQA METHODS

Table 1 shows the summary of recent conventional PPG-SQA methods available in the literature. To enhance the PPG

**TABLE 1. Summary of existing conventional (non-DL) PPG-SQA methods.**

| Performance of non-DL-based PPG-SQA Methods | | | | | | |
|---|---|---|---|---|---|---|
| Database | Method | Segment Duration (sec) | Performance | | | Real-Time (Yes/No) |
| | | | SE(%) | SP(%) | ACC(%) | |
| CSL, MIMIC-II, MIT-BIH SLP, Wrist, Cup, In-house | Five Hierarchical Decision Rules, Two Amplitude and Prediction Coefficient Features (2020) [14] | 5 | 98.22 | 90.71 | 93.21 | Yes |
| | SVM (RBF(C=100, gamma=0.5)) (2020) [14] | | 98.22 | 88.59 | 91.80 | |
| | SVM (Linear(C=100)) (2020) [14] | | 98.39 | 87.85 | 91.36 | |
| | Kurtosis (2020) [14] | | 77.48 | 35.13 | 49.24 | |
| | Shannon Entropy (2020) [14] | | 79.45 | 23.62 | 42.23 | |
| | Shannon Entropy and Kurtosis (2020) [14] | | 67.29 | 25.21 | 39.24 | |
| | Fiducial Features (2020) [14] | | 78.00 | 72.22 | 74.13 | |
| CSL, MIMIC-II, MIT-BIH SLP, In-house | Hierarchical Decision Rules with Amplitude and Autocorrelation Features (2019) [16] | 5 | 99.29 | 95.31 | 97.76 | Yes |
| | Fiducial Features (2019) [16] | | 90.89 | 69.93 | 82.82 | |
| | Statistical Features (2019) [16] | | 71.61 | 52.51 | 64.28 | |
| In-house | Decision tree (2019) [47] | 20 | 88.96 | 86.30 | NR | No |
| | SVM (2019) [47] | | 93.25 | 91.90 | NR | |
| | Threshold Optimized (2019) [47] | | 90.05 | 89.48 | NR | |
| | Ensembelled Decision Tree (2019) [47] | | 91.56 | 91.97 | NR | |
| | Template Matching and Threshold-based Rules (2015) [48] | 60 | 91.00 | 95.00 | NR | No |
| | Shannon entropy (0.8) (2011) [49] | 10 | 85.00 | 99.40 | 87.40 | Yes |
| | kurtosis (3.5) (2011) [49] | | 72.60 | 98.60 | 77.00 | |
| | Fusion Detection (2011) [49] | | 86.90 | 98.30 | 88.80 | |

CSL:Complex System Laboratory; MIT-BIH SLP: MIT-BIH Polysomnographic; MIMIC-II: Multiparameter Intelligent Monitoring in Intensive Care II; BIDMC: Beth Israel Deaconess Medical; RBF: Radial Basis Function; SVM: Support vector Machine; NR: Not Reported

signal quality, several signal processing techniques have been implemented to eliminate the low and high-frequency components or motion artifacts in [47], [50], and [51]. The frequency and time domain features were extracted and used as states in a Gaussian filter [52], template matching and threshold-based techniques [48] to accept or reject signals based on their quality. In some of the methods, features obtained from pre-processed signals are given as input to the machine learning (ML) algorithms such as decision tree (DT) [50], K-nearest neighbors (KNN), Naive Bayesian classifier (NB), logistic regression (LR), random forest (RF), to classify the quality of the PPG signal. S. Vadrevu et al. [16] presented an SQA method based on amplitude and autocorrelation function (ACF) features that can differentiate between acceptable and unacceptable signals. G. N. K Reddy et al. [14] proposed an SQA method based on five hierarchical decision rules using three features comprising two amplitude features and one prediction coefficient. M. Elgendi [53] extracted several indexes to classify the low and high-quality PPG signals using a support vector machine (SVM). However, some of these methods cannot be applied in real-time due to their complexity and constraints to achieve the desired results. Therefore, in recent years, researchers have been exploring deep-learning (DL) neural networks that can take raw signals directly as input and automatically classify the signal quality.

### B. DL-BASED PPG SQA METHODS

In the literature, various quality-aware DNN architectures were used to classify the clean and noisy PPG segments. Liu et al. studied the quality assessment of PPG signal to improve the $SPO_2$ detection accuracy using SVM and 2D-CNN (VGG-19) models. The 12 PPG signal quality index (SQI) features were extracted and given as input to the SVM and VGG-19 models, resulting in an accuracy of $89.5 \pm 3.87\%$ and $86.2 \pm 4.28\%$, respectively [6]. The PPG signal quality was assessed using traditional CNNs such as VGG-19 and ResNet-50, resulting in an accuracy of 89.50% and 92.50%, respectively [54]. Pereira et al. presented a DNN-based PPG SQA method to enhance atrial fibrillation detection accuracy. This method contains traditional neural network architecture (ResNet-18) and achieved an accuracy of 98.50%, specificity of 97.90%, and sensitivity of 98.80% [55]. Although conventional DNN architectures can achieve high PPG classification accuracy, they increase the computational load and reduce the battery lifetime of PPG

analysis devices. Due to resource-constrains of continuous health monitoring devices, the above-mentioned conventional deep neural network methods were difficult to implement in real-time computing platforms [6], [54], [55].

Jianzhong et al. converted time-series 10-sec PPG segments into time-frequency spectral images using short-time Fourier transform (STFT). The PPG image spectrums were fed into a 2D-CNN model to classify clean and noisy time-frequency PPG spectrum. The method was tested using the vitalDB database and achieved an ACC of 98.30%, SE of 98.90%, and SP of 96.70% [13]. Filipa et al. presented the PPG waveform quality using various DNNs to identify the best-fit model. The synchrosqueezed Fourier transform (SSFT) was applied to the PPG signal and fed as input to 2D-DNN algorithms. The CNN-LSTM deep neural network algorithm outperforms other models and achieved an accuracy of 89.40% [56]. Chatterjee et al. developed a 7-layer 2D-CNN architecture to classify the clean and noisy PPG time-frequency spectrums. The PPG time-frequency spectral images were obtained using a quantum pattern recognition algorithm. Further, the 2D-CNN architecture was tested using the University of Queensland (UQ) database, resulting in an ACC of 98.30%, an SE of 99.30%, and an SP of 94.50%, [40]. Roh and Shin developed a 2-layer 2D-CNN architecture to classify the clean and noisy PPG 2D images. The 2-layer CNN model had an ACC of 97.50%, SE of 96.40%, and SP of 98.70% [41].

Kasaeyan et al. developed an automatic clean and noisy 60-second PPG segment classification using deep 1D-CNN architectures. The 1D-CNN model was evaluated using an in-house database and achieved a sensitivity of 83.33% and specificity of 83.54% [1]. Goh et al. presented the 13-layer 1D-CNN with a non-linear activation function (ReLU) to automatically classify the clean and noisy 5-sec PPG segments. The 1D-CNN model was tested using MIMI-II and in-house databases and achieved an ACC of 94.50% [17]. Aliamiri et al. studied the 30-sec clean and noisy PPG segments classification analysis using the 3-layer deep 1D-CNN model. The method achieved a classification accuracy of 90.52% [57]. Serena et al. studied the classification of 1-sec acceptable and unacceptable quality PPG signals using 4-layer 1D-CNN architecture (32 filter and ReLU activation function). The PPG signals were tested using two different databases and had accuracies of 86% and 81%, respectively [58]. Sivanjaneyulu et al. studied the 2 and 4-layer and three kernels (16, 32, and 64) with only ReLU activation function 1D-CNN architecture to assess the quality of the PPG signal. The method was tested using three different databases (DB1 (NF-PPG vs WC-PPG), DB2 (NF-PPG vs SYN-RN-PPG), and DB3 (NF-PPG vs SYN-ACCE-PPG)). The optimal 4-layer with 32 filters achieved an ACC of 99.58% for DB1, 99.99% for DB2, 75.80% for DB3 [59]. Further, raw PPG signals were compressed using five different CS matrices with CR of 2 given as input to the 1D-CNN model (4)-layer, 32 filter, and ReLU) to assess the quality of the compressed PPG signal. The method achieved an ACC of 99.55% for DB1, 99.99% for DB2, and 72.71% for DB2 [60]. Khan et al. extracted the Horizontal Visibility Graph (HVG) and Neighbour Edge Restricted Horizontal Visibility Graph (NERHVG) network from the clean and noisy PPG signals and fed them into machine learning algorithms to perform the quality assessment. Among the two aforementioned networks, NERHVG shows superior results to HVG and achieved 99.09%, 95.03%, 96.56%, and 84.63% on different databases using the Gaussian Naive Bayes classifier [61]. Priyanka et al. studied graph neural network-based PPG signal quality assessment using ML algorithms and CNN architecture. The method was tested using standard databases and achieved an accuracy of 99.23% and 99.21% for CNN architecture and Naive Bayes algorithms [62].

The non-traditional 1D and 2D-DNN methods were not explored using different non-linear activation functions, layers, and kernels. Most of the existing methods were evaluated using longer-duration PPG signals to classify the clean and noisy segments; however, many clean PPG signals with a shorter duration of noise were eliminated. The existing methods were not evaluated using unknown databases, which is important to know the reliability and robustness of the method. Computational complexity and real-time implementation of existing 1D and 2D-CNN methods were not addressed, which are important to know the real-time feasibility of the method [1], [13], [17], [40], [56], [57], [58].

In the past studies on PPG signal quality assessment methods, the features and heuristic decision rules or deep models were developed with limited variations in PPG noises, which did not include different levels and patterns of motion artifacts and varying levels of random noises and also different normal and abnormal PPG waveform patterns. Thus, it limits the application of existing methods in checking the quality of PPG signals which are corrupted with various kinds of noises and artifacts having different levels of amplitude. Further, the performance of existing methods was not evaluated using untrained standard databases which are used for blood pressure estimation, respiration rate, sleep apnea detection, pulse rate variability analysis, and pulse rate estimation to demonstrate achieving better accuracy under varying patterns of PPG signals and artifacts. Our prior work in [59] and [63] reveals that proper selection of the neural network hyper-parameters would improve the performance of the 1D-CNN based derivative PPG SQA. Although some of the existing DL-based PPG SQA methods had better accuracy, they were not implemented in real-time platforms, computational complexity is not reported by choosing the best non-linear activation function, number of layers, and number of kernels.

In this work, we developed derivative PPG-based various 1D-CNN models (27 in number) by tuning different hyper-parameters namely the number of layers, kernels, and activation functions to select the best hyper-parameters to

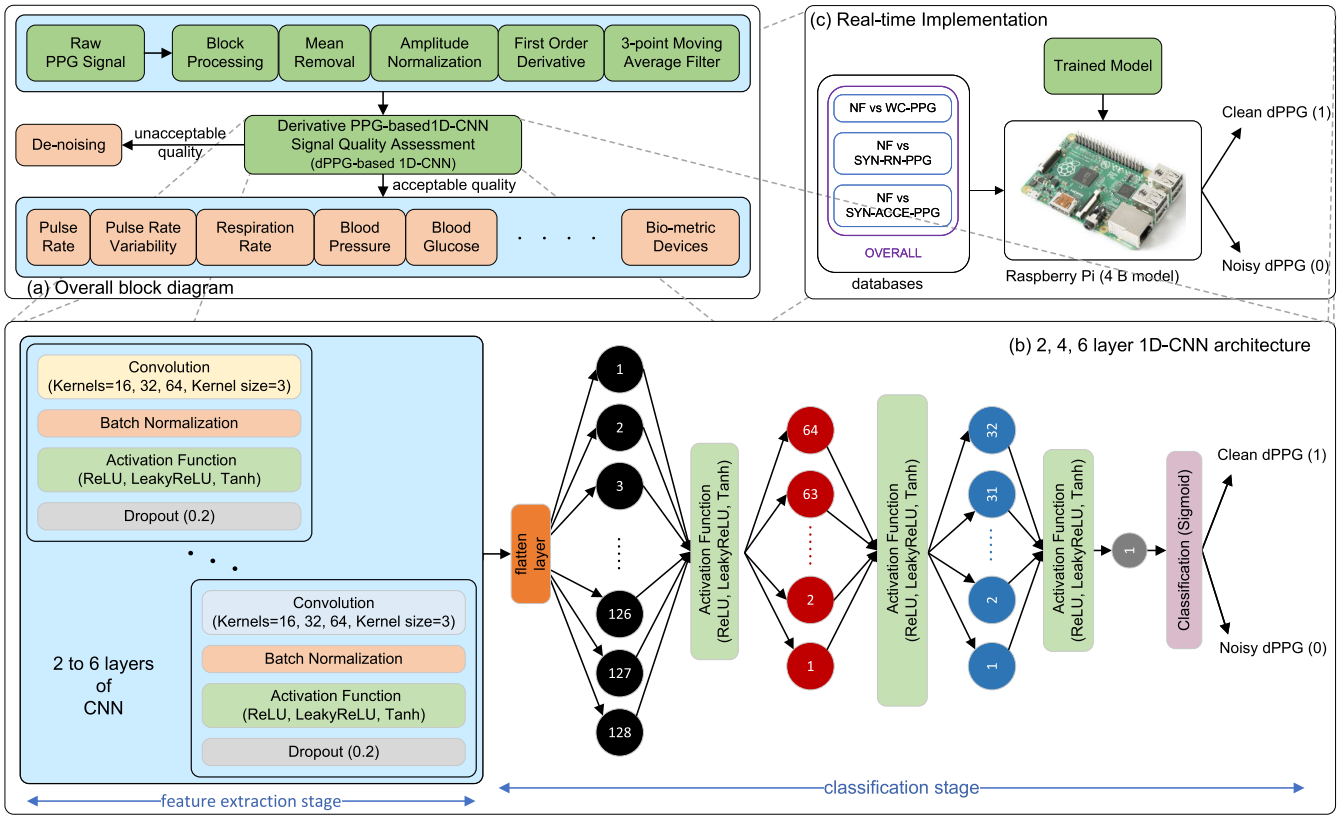


**FIGURE 3.** (a) Overall block diagram of the derivative PPG-based 1D-CNN SQA method, (b) 2, 4 and 6 layer 1D-CNN architectures, (c) shows the implementation of 1D-CNN-based dPPG-SQA method using real-time computing platform.

automatically classify the clean and noisy PPG segments, which were not addressed in the literature. The optimal model plays a crucial role in not only improving the classification accuracy but also reducing the latency and model size which are most important for health and fitness monitoring devices.

## III. PROPOSED METHOD

Fig. 3 summarizes the overall block diagram of the dPPG-based 1D-CNN-SQA method. The raw PPG signals were collected from various databases with different sampling rates. The collected PPG signals were resampled with a sampling rate of 125 Hz, block processed with 375 samples (3 seconds), mean is removed, and amplitude is normalized, see Fig. 3(a). Further, the normalized PPG segment is fed into a first-order derivative system and then followed by a 3-point moving average filter to smooth the high-frequency components present in the derivative PPG signal. The smoothed derivative PPG signal is fed into a 1D-CNN architecture to automatically classify the quality. The acceptable quality derivative PPG signals would be used to measure the vital sign parameters, which reduces the false alarms [16]. The unacceptable quality derivative PPG signals were either de-noised or discarded as shown in Fig. 3(a).

In this study, we explored the layer optimization technique, which is used to improve the performance and efficiency of deep learning models [41]. In general, deep learning models include a multiple number of layers, each layer in the model includes different sub-layers and hyperparameters [64]. The selection of sub-layers and hyperparameters plays a crucial role for layer optimization [65]. The optimal selection of sub-layers and hyperparameters is identified by using the hit-and-trial method. In this work, we have chosen 1D-CNN architecture to automatically extract the most prominent features from the input signals. The CNN architecture consists of CLs followed by an activation function, a flatten layer, a fully connected dense layer, and a classification layer to classify the clean and noisy segments, see Fig. 3. The working principle of each CL is that it will extract features by performing the convolution between the input signal and filter weights. Mathematically convolution operation can be written as below in the context of 1D-CNN architecture [63].

$$y_{i+1}^{j} = x_j^i \cdot w_j^i + B_j^i \tag{1}$$

where $w_j^i$, $B_j^i$, and $x_j^i$ represent trainable weights, bias, and input, respectively for the $j^{th}$ kernel of $i^{th}$ convolutional layer.

The CL output is given as input to the activation function, which plays a crucial role due to its nonlinear property, making the model fit non-linear data. In the proposed method, we selected the three most important activation functions such as ReLU, LeakyReLU, and Tanh to identify the optimal activation function [58]. In the classification

stage, the sigmoid activation function [58] is used to perform the stratification of the clean and noise PPG segments.

The CNN architectures consist of a classification stage, which includes a flatten layer, dense layers, and a classification layer, see Fig. 3(b). The classification layer predicts the quality of the signal (clean (1) or noise (0)) using the sigmoid activation function by taking the preceding layers' output as input. In this study, we considered 2, 4, and 6-layer 1D-CNN architectures with 16, 32, and 64 kernels using ReLU, LeakyReLU, and Tanh activation functions, see Fig. 3(b). The proposed method consists of 2, 4, and 6-layer CNN architectures with kernels 16, 32, and 64 and ReLU, LeakyReLU, and Tanh activation functions. The method was evaluated using three clean and noise dPPG segments: NF versus WC-PPG, NF versus SYN-RN-PPG, and NF versus SYN-ACCE-PPG. The feature extraction stage of 1D-CNN architectures includes 2, 4, and 6 layers; each layer includes the same number of sub-layers, such as the convolutional layer, batch normalization, activation function, and dropout (0.2), see Fig. 3(b). The output of the last dropout layer is given to the flatten layer to change the dimensions, see Fig. 3(b). The flatten layer output is applied to 4 fully connected dense layers with 128, 64, 32, and 1 neurons, respectively. The final dense layer output is given to the sigmoid function to classify the derivative PPG signal into a clean dPPG (acceptable) or a noisy dPPG (unacceptable). The above proposed 2, 4, and 6 CL layers were trained using various model hyper-parameters: binary cross entropy (BCE(loss function)), adaptive movement estimator (Adam(optimizer)), 0.001 (step size/learning rate), batch size (10), and epochs (20), see Table 2 for more details.

### A. EVALUATION METRICS

In existing PPG-SQA methods, the evaluation results were computed using the following parameters: *true positive (TP)*, *false negative (FN)*, *false positive (FP)*, and *true negative (TN)*. By using these four parameters, the following evaluation metrics are computed: The *sensitivity (SE)* [13], [40], [55] is defined as the percentage of correctly classified clean segments. Mathematically, sensitivity can be computed as:

$$\mathrm{SE} = \frac{\mathrm{TP}}{\mathrm{TP} + \mathrm{FN}} \times 100\ \% \tag{2}$$

The *specificity (SP)* [13], [40], [55] is defined as the percentage of correctly classified noisy segments. Mathematically, specificity can be computed as:

$$\mathrm{SP} = \frac{\mathrm{TN}}{\mathrm{TN} + \mathrm{FP}} \times 100\ \% \tag{3}$$

The *Accuracy (ACC)* [13], [55], [56], [58] is defined as the total percentage of correctly classified clean and noisy segments. Mathematically, accuracy can be computed as:

$$\mathrm{ACC} = \frac{\mathrm{TP} + \mathrm{TN}}{\mathrm{TP} + \mathrm{TN} + \mathrm{FN} + \mathrm{FP}} \times 100\ \% \tag{4}$$

**TABLE 2. Hyper-parameters and database used for the derivative PPG-based 1D-CNN SQA method.**

| Dataset and Parameters | Information/Specification |
|---|---|
| Dataset Format | .mat, csv |
| Sampling rate of the PPG signal | 125 Hz |
| Total training dPPG segments: | 494486 |
| Known database test dPPG segments: | 68540 (NF versus WC-PPG),<br>317400 (NF versus SYN-RN-PPG),<br>126960 (NF versus SYN-ACCE-PPG) |
| Unseen database test dPPG segments: | 15000 (clean) vs 3339 (noise) from UCI,<br>6938 (clean) vs 1858 (noise) from VitalDB,<br>30000 (clean) vs 1920 (noise) from PulseDB |
| Duration of the PPG segment | 3 sec |
| Number of layers | 2, 4, and 6 |
| Number of BN layers | 2 for 2 layer, 4 for 4 layer,<br>and 6 for 6 layer |
| Total number of dropout layers | 2 for 2 layer (0.2), 4 for 4 layer (0.2),<br>and 6 for 6 layer (0.2) |
| Total number of fully connected layers | 4 |
| Non-linear AFs | ReLU, LeakyReLU, Tanh |
| Classification layer | Sigmoid |
| Batch size | 10 |
| Step size/Learning rate | $10^{-}3$ |
| Optimizer | Adam |
| Epochs | 20 |
| Loss function | BCE |
| Kernel size | $1\times3$ |
| No. of filters | 16, 32, 64 |

## IV. NOISE-FREE AND NOISY PPG SIGNAL DATABASES: DESCRIPTION AND IMPLEMENTATION PLATFORM

The proposed derivative-based 1D-CNN PPG-SQA method is validated using 7 trained (known) and 3 untrained (unknown/unseen) databases, which are summarized below:

MIT-BIH Polysomnographic Database [66]: The database includes recordings of various physiological signals during sleep from subjects aged 32 to 56. Specifically, the PPG records "slp01a" and "slp01b" are segments from one subject's polysomnogram, separated by an hour, while "slp02a" and "slp02b" are segments from another subject, separated by ten minutes. These signals were digitized with a sampling frequency of 250 Hz and a resolution of 12 bits per sample.

Medical Information Mart for Intensive Care and MIMIC-III Database [67], [68]: The database contains recordings from patients aged 16 and above, with each patient having multiple recordings that can range from a few seconds (usually anomalies) to several hours. It includes various physiological signals, such as PPG and ABP, recorded at a sampling rate of 125 Hz. The data covers different heart rhythms and conditions, including normal sinus rhythm (NSR), premature atrial and ventricular contractions (PAC/PVCs), atrial fibrillation (AF), and other signal patterns.

Beth Israel Deaconess Medical Center Database [69]: The BIDMC database consists of 53 recordings, each lasting 8 minutes, capturing ECG, PPG, and thoracic impedance (reference) respiratory signals. These signals were collected

from critically ill patients (median age: 64.81, ranging from 19 to 90+, with 32 females and 21 males) during hospital care and digitized at a sampling rate of 125 samples per second. The BIDMC database is extensively used to evaluate the performance of algorithms designed to estimate respiratory or breathing rates from PPG signals.

Wrist Database [70]: The wrist database was collected from eight participants (3 males, 5 females) aged 22 to 32 years (mean age 26.5 years) during various physical activities, including biking, walking, and treadmill running at different speeds and time intervals. The signals were digitized at a sampling rate of 256 Hz.

Cup Database [71]: The IEEE Signal Processing Cup 2015 database includes PPG signals recorded from the wrist using a pulse oximeter with a green LED (609 nm) and three-axis accelerometer signals. The data were collected from 12 male subjects with yellow skin tones, aged 18 to 35 years. All signals were digitized at a sampling rate of 125 Hz.

Complex System Laboratory Database [72]: The CSL database includes six 60-minute manually annotated recordings from six patients, acquired using a data acquisition system in the Complex Systems Laboratory (CSL). These recordings, sampled at 125 Hz, were band-pass filtered and auto-scaled. The database contains manual beat annotations from two independent experts as well as automatic annotations generated by the CSL reference algorithm.

CapnoBase Database [72]: The CapnoBase database contains six datasets with annotated respiratory signals, including respiratory flow, pressure, and PPG signals recorded from anesthesia monitors during elective surgeries involving 59 children and 35 adults under general anesthesia. The PPG recordings were digitized at a sampling rate of 300 Hz, with each beat manually annotated by an expert using the CapnoBase Signal Evaluation Tool. Experts also labeled the beginning and end of all visual artifacts in the PPG waveforms. This database is widely used for evaluating respiration rate estimation from PPG signals.

University of California Irvine (UCI) Database [73]: The MIMIC-II database consists of a large number of subjects, with different physiological, pathological, and morphological signal variations. The MIMIC-II database includes various biosignals with a sampling rate of 125 Hz and a resolution of 8-bit. The signals were recorded from the intensive care patients. Further, the MIMIC-II database was preprocessed, creating the UCI database. The UCI database consists of 12000 subjects with different signal durations. The UCI database includes preprocessed ECG, PPG, and ABP signals with a sampling rate of 125 Hz and a resolution of 8 bits. The signals were recorded from the intensive care patients.

VitalDB Database [74]: The database comprises 6388 surgical patients aged between 35 and 72 years, containing intraoperative biosignals and clinical data. The information was collected from patients undergoing non-cardiac surgeries (including general, thoracic, urologic, and gynecologic procedures) at Seoul National University Hospital in Seoul, Republic of Korea. The dataset features various lengths of PPG signals, with a sampling rate of 500 Hz, alongside ECG and BP signals, all acquired using the ''TramRac-4A'' device.

PulseDB Database [75]: PulseDB is a comprehensive and curated dataset derived from the MIMIC-III matched subset and the VitalDB databases. The MIMIC-III matched subset includes 22317 records from 10282 patients who were admitted to the critical care unit (ICU) at Beth Israel Deaconess Medical Center. The VitalDB database features 6388 records from 6090 ICU patients who underwent surgeries at Seoul National University Hospital. Both databases contain simultaneously recorded ECG (lead II), PPG (fingertip), and ABP signals. PulseDB includes 10-second segments from a total of 10 hours of data across 5,361 subjects (average age: $60.87 \pm 15.58$). This data is sourced from 4941 records from the MIMIC-III matched subset and 3458 records from the VitalDB database, all digitized at a sampling rate of 125 Hz.

In-house Database (IITBBS) [14]: The in-house finger pulse PPG database was gathered from 20 volunteer subjects at rest, including 12 females and 8 males aged 18 to 35 years. PPG signals were recorded for 10 to 15 minutes using three different commercially available devices: the Texas Instruments Pulse Oximeter Medical Development Kit, the BioRadio physiological monitoring system, and a real-time finger pulse sensor interfaced with Arduino. These signals were then resampled to a frequency of 125 Hz.

To perform the proposed derivative PPG-quality assessment method, several clean and noisy pathological/morphological PPG segments are taken from the aforementioned standard databases. Table 3 provides the number of clean and noise segments taken from some of the aforementioned original seven standard databases and one in-house database (trained/known database) to evaluate the performance of the proposed method. The seven standard databases include MIT-BIH SLP (21420 clean PPG), MIMIC (3720 clean PPG), BIDMC (8480 clean PPG), MIMIC-III (8360 clean PPG), capnobase (6720 clean PPG), CSL (2360 clean PPG), and wrist-cup (5060 noise PPG). The

**TABLE 3. Summary of standard and in-house database used to evaluate the derivative PPG-based 1D-CNN-SQA method.**

| Name of Database | Number of Segments | Sampling Rate (Hz) | Type of Abnormal PPG | Recording Type | Presence of Noise | Noise Type |
|---|---|---|---|---|---|---|
| MIT-BIH SLP [66] | 21420 | 250 | NR | Normal | NR | NR |
| MIMIC [67] | 3720 | 125 | NR | Normal | NR | NR |
| BIDMC [69] | 8480 | 125 | NR | Normal | NR | NR |
| MIMIC-III [68] | 8360 | 125 | AF,PAC/PVC Events | Normal | NR | NR |
| CapnoBase [72] | 6720 | 300 | NR | Normal | NR | NR |
| CSL [72] | 2360 | 125 | NR | Normal | NR | NR |
| IITBBS [14] | 12420 | 125 | NR | Normal | NR | NR |
| Wrist [70]-cup [71] | 5060 | 256 | NR | Normal | Yes | MA |

MA: Motion Artifact; PVC: Premature Ventricular Contractions; AF: Atrial Fibrillation; PAC:Premature Atrial Contraction

in-house database consists of 12420 clean PPG segments. A total of 63480 clean PPG segments (3174 60-second PPG segments) with different amplitude morphology and 5060 noisy PPG segments (253 60-second PPG segments) with each PPG segment duration of 3 seconds. The first 30-second 3174 clean PPG segments (31740 3-second clean PPG segments) and 60-second 253 noisy PPG segments (5060 3-second noisy PPG segments) were used to train the proposed 1D-CNN models. Since deep learning architectures achieve better performance using large training datasets, a huge dataset is considered for training the proposed CNN models. To achieve the large training set, the clean 31740 3-second PPG segments were overlapped with 330 samples (238050 3-second clean PPG segments). Similarly, the two noisy PPG segments were synthetically generated by adding normalized 3-second acceleration and random signals with different amplitude levels (0.3, 0.5, 0.7, and 0.9) to the clean 31740 3-second PPG segments, achieving 126960 acceleration noise affected and 126960 random noise affected PPG-segments. Thus, the training dataset includes 238050 overlapped 3-second clean and 258980 3-second noisy PPG segments, a total of 497030 3-second PPG segments (80% were used for training the model and 20% validation).

Similarly, the test dataset (known dataset) includes a total of 63480 3-second clean segments (NF-PPG), which are added to acceleration signal with two amplitude levels (0.7, and 0.9) and a random signal with four amplitude levels (0.3, 0.5, 0.7 and 0.9), achieved 126960 acceleration noise affected (SYN-ACCE-PPG) and 253920 random noise affected (SYN-RN-PPG) PPG-segments. The optimal model was also tested using three unseen datasets such as UCI, VitalDB, and PulseDB to know the robustness of the method. Three 60-sec PPG segments were taken from different databases (MIT-BIH SLP, CSL, and wrist-cup) and evaluated the derivative PPG-SQA output using the optimal model as shown in Fig. 4. The proposed method was developed using the Python Jupyter Notebook IDE software with version 3.3.1, which has in-built DNN libraries such as Matplotlib, Sklearn, Pandas, Numpy, Keras, and TensorFlow to perform the back-end computations. The computing platform is the Intel Xeon (R) E52620 CPU running at 2.40 GHz, with 40 GB RAM.

## V. RESULTS AND DISCUSSION

Table 4 summarizes the evaluation results of 2, 4, and 6-layer CNN architectures in terms of activation functions (ReLU and LeakyReLU and Tanh), number of kernels (16, 32, and 64), model size (MS), and training parameters. The proposed dPPG-based 1D-CNN-SQA method was investigated using performance metrics such as sensitivity, specificity, and accuracy. However, in existing methods, the performance was evaluated using a single-noise dataset with a smaller number of segments. Therefore, we have collected and created three kinds of noisy PPG segments such as WC-PPG, SYN-RN-PPG, and SYN-ACC-PPG. The main aim of this study is to identify the optimal-trained model to classify the acceptable and unacceptable derivative PPG segments.

The proposed method shows better results for a 6-layer 1D-CNN with 32 kernels using the ReLU activation function, see Table 4. It achieves 99.84% of SE, 97.94% of SP, and 99.70% of ACC for noise-free versus WC-PPG; 99.79% of SE, 100.00% of SP, and 99.96% of ACC for noise-free versus SYN-RN-PPG; 84.48% of SE, 74.63% of SP, and 78.17% of ACC for noise-free versus SYN-ACCE-PPG. For overall database,[1] 99.16% of SE, 79.22% of SP, and 88.82% of ACC is achieved as shown in Table 4. The optimal 6-layer CNN architecture has a memory size of 18.9 MB and a total of 1,558,433 trainable parameters. The performance results show that choosing the right number of convolutional layers and optimizing the CNN parameters are two of the most important things that can be done to improve accuracy while reducing computational load. This is particularly important for wearable devices with limited resources.

Table 5 summarizes the performance of our previous work (1D-CNN-based raw PPG-SQA) and proposed work (1D-CNN-based derivative PPG-SQA). The above methods has their own significance in extracting the vital sign parameters. The main objective of the raw and derivative quality assessment works is to find the optimal parameters of the 1D-CNN architectures to achieve superior performance. The 1D-CNN-based raw PPG-SQA method was trained and tested using 2 and 4 layers with 16, 32, and 64 filters using the only ReLU activation function to find the optimal parameters [59], and it achieved better performance for 4 CLs and 32 kernels as shown inTable 5. While this approach provided valuable insights, it was limited by the simplicity of the 1D-CNN architecture. The proposed work is extended by enhancing the 1D-CNN architecture to improve the accuracy and robustness of PPG-SQA under various noise conditions. Specifically, we increased the number of layers (to 2, 4, and 6) and introduced additional activation functions (ReLU, LeakyReLU, and Tanh) while maintaining the same kernel sizes (16, 32, and 64), and achieved better performance for 6-layer and 32 kernels with ReLU activation function. This extended architecture allows us to identify the optimal parameters and model configuration for derivative PPG SQA to accurately assess the clean and noise derivative segments. Moreover, the proposed method is implemented on a real-time computing platform, such as the Raspberry Pi, to verify its feasibility in real-time applications, which is not addressed in the raw PPG-SQA method. This implementation demonstrates the practical applicability of our method, which is a crucial step towards real-world deployment. Further, the optimal model (6-layer and 32 kernel with ReLU) is validated using three unseen databases (UCI, VitalDB, and PulseDB), which is not addressed in the 1D-CNN raw PPG-SQA method.

[1]It contains all databases, i.e., WC-PPG, SYN-RN-PPG, SYN-ACCE-PPG, and NF.

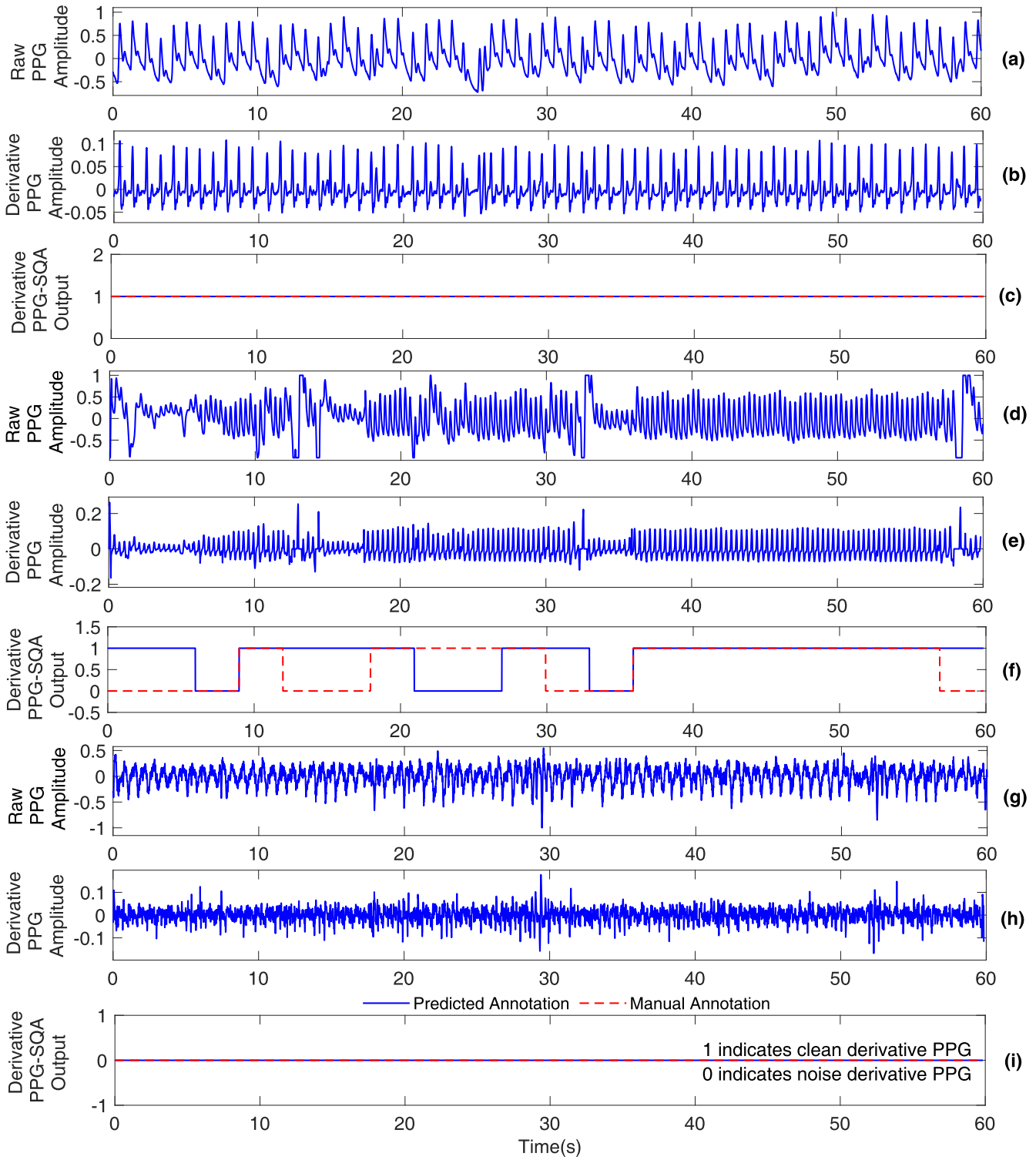


**FIGURE 4.** Derivative PPG-SQA output for different morphological and motion artifact affected segments using optimal CL (6-layer). The original PPG signals are shown in (a), (b), and (c), which are taken from MIT-BIH SLP (record name: SLP14), CSL database (record name: POX1) and wrist database (record name: s4run), respectively, their corresponding derivative PPG signals are shown in (b), (e), and (h), and their corresponding derivative PPG-signal quality output is shown in (c), (f), and (i).

### A. COMPUTATIONAL COMPLEXITY ANALYSIS

Though many PPG-SQA methods exist in the literature, computational complexity analysis was not reported, which is one of the most important parameters to verify the real-time feasibility of the method. The best-trained model may reduce energy consumption, computational load, and

**TABLE 4. Performance of 2, 4, and 6 layers derivative PPG-based 1D-CNN-SQA method in terms of benchmark metrics, activation functions, and number of filters for clean vs noisy dPPG segments from various databases.**

| Activation Function | No. of filters | NF versus Noisy PPG Segments | Performance of 2- Layer | | | | | Performance of 4- Layer | | | | | Performance of 6- Layer | | | | |
|---|---|---|---|---|---|---|---|---|---|---|---|---|---|---|---|---|---|
| | | | SE (%) | SP (%) | ACC (%) | MS (MB) | Training Parameters | SE (%) | SP (%) | ACC (%) | MS (MB) | Training Parameters | SE (%) | SP (%) | ACC (%) | MS (MB) | Training Parameters |
| ReLU | 16 | NF vs WC-PPG | 99.85 | 90.12 | 99.17 | 9.0 | 777361 | 94.17 | 97.76 | 94.42 | 9.0 | 778993 | 98.61 | 96.83 | 98.49 | 9.5 | 780625 |
| | | NF vs SYN-RN-PPG | 99.84 | 100.00 | 99.96 | | | 94.31 | 100.00 | 98.81 | | | 98.40 | 100.00 | 99.67 | | |
| | | NF vs SYN-ACCE-PPG | 72.29 | 72.45 | 72.39 | | | 79.41 | 71.00 | 74.02 | | | 63.38 | 79.41 | 73.65 | | |
| | | Overall | 99.71 | 71.68 | 85.17 | | | 99.46 | 71.45 | 84.93 | | | 92.58 | 79.01 | 85.54 | | |
| | **32** | **NF vs WC-PPG** | 99.37 | 92.34 | 98.87 | 17.7 | 1545761 | 98.78 | 96.91 | 98.65 | 17.8 | 1552097 | **99.84** | **97.94** | **99.70** | **18.9** | **1558433** |
| | | **NF vs SYN-RN-PPG** | 99.45 | 99.56 | 99.54 | | | 98.81 | 100.00 | 99.75 | | | **99.79** | **100.00** | **99.96** | | |
| | | **NF vs SYN-ACCE-PPG** | 72.64 | 56.53 | 62.32 | | | 65.57 | 86.00 | 78.66 | | | **84.48** | **74.63** | **78.17** | | |
| | | **Overall** | 99.38 | 68.01 | 83.11 | | | 92.74 | 72.20 | 82.09 | | | **99.16** | **79.22** | **88.82** | | |
| | 64 | NF vs WC-PPG | 98.33 | 96.27 | 98.18 | 35.4 | 3087169 | 89.72 | 99.31 | 90.39 | 35.7 | 3112129 | 98.53 | 98.55 | 98.53 | 37.8 | 3137089 |
| | | NF vs SYN-RN-PPG | 98.57 | 100.00 | 99.70 | | | 89.12 | 100.00 | 97.73 | | | 98.81 | 100.00 | 99.75 | | |
| | | NF vs SYN-ACCE-PPG | 49.84 | 80.41 | 69.43 | | | 43.96 | 94.12 | 76.10 | | | 47.60 | 70.05 | 61.99 | | |
| | | Overall | 99.73 | 78.17 | 87.43 | | | 72.67 | 90.98 | 82.16 | | | 98.95 | 82.23 | 90.28 | | |
| LeakyReLU | 16 | NF vs WC-PPG | 97.35 | 98.77 | 97.45 | 9.0 | 777361 | 89.10 | 99.01 | 89.80 | 9.0 | 778993 | 94.94 | 96.87 | 95.07 | 9.5 | 780625 |
| | | NF vs SYN-RN-PPG | 97.56 | 100.00 | 99.49 | | | 91.59 | 100.00 | 98.25 | | | 95.84 | 100.00 | 99.14 | | |
| | | NF vs SYN-ACCE-PPG | 61.01 | 48.50 | 79.84 | | | 70.45 | 94.55 | 85.89 | | | 85.62 | 90.77 | 88.92 | | |
| | | Overall | 95.77 | 73.88 | 84.42 | | | 83.02 | 79.32 | 81.10 | | | 94.68 | 73.92 | 83.91 | | |
| | 32 | NF vs WC-PPG | 95.09 | 95.53 | 95.12 | 17.7 | 1545761 | 86.89 | 97.70 | 87.65 | 17.8 | 1552097 | 96.22 | 98.89 | 96.40 | 18.9 | 1558433 |
| | | NF vs SYN-RN-PPG | 95.80 | 100.00 | 99.12 | | | 89.35 | 100.00 | 97.79 | | | 97.02 | 100.00 | 99.38 | | |
| | | NF vs SYN-ACCE-PPG | 74.26 | 90.06 | 84.39 | | | 97.21 | 90.95 | 93.20 | | | 61.42 | 90.57 | 80.10 | | |
| | | Overall | 95.48 | 73.52 | 84.09 | | | 96.78 | 71.25 | 83.53 | | | 96.97 | 77.76 | 87.01 | | |
| | 64 | NF vs WC-PPG | 91.78 | 90.81 | 91.72 | 35.4 | 3087169 | 90.45 | 98.18 | 90.99 | 35.7 | 3112129 | 99.51 | 96.51 | 99.30 | 37.8 | 3137089 |
| | | NF vs SYN-RN-PPG | 92.73 | 99.98 | 98.48 | | | 92.58 | 100.00 | 98.46 | | | 99.58 | 100.00 | 99.91 | | |
| | | NF vs SYN-ACCE-PPG | 86.38 | 87.80 | 87.29 | | | 73.35 | 93.69 | 86.39 | | | 70.71 | 72.32 | 71.74 | | |
| | | Overall | 97.23 | 68.96 | 82.57 | | | 93.04 | 73.75 | 83.03 | | | 99.42 | 73.24 | 85.85 | | |
| Tanh | 16 | NF vs WC-PPG | 99.02 | 95.75 | 98.79 | 9.0 | 777361 | 97.93 | 95.12 | 97.73 | 9.0 | 778993 | 97.50 | 91.25 | 97.06 | 9.5 | 780625 |
| | | NF vs SYN-RN-PPG | 98.69 | 100.00 | 99.72 | | | 97.45 | 100.00 | 99.46 | | | 97.15 | 100.00 | 99.41 | | |
| | | NF vs SYN-ACCE-PPG | 74.04 | 83.02 | 79.80 | | | 49.65 | 79.55 | 68.80 | | | 76.37 | 87.84 | 83.72 | | |
| | | Overall | 97.05 | 80.75 | 88.60 | | | 94.14 | 83.20 | 88.46 | | | 95.33 | 83.30 | 89.09 | | |
| | 32 | NF vs WC-PPG | 96.63 | 95.75 | 96.56 | 17.7 | 1545761 | 98.53 | 96.05 | 98.35 | 17.8 | 1552097 | 95.91 | 94.25 | 95.80 | 18.9 | 1558433 |
| | | NF vs SYN-RN-PPG | 96.87 | 100.00 | 99.35 | | | 97.97 | 100.00 | 99.57 | | | 95.55 | 100.00 | 99.08 | | |
| | | NF vs SYN-ACCE-PPG | 60.35 | 84.43 | 75.78 | | | 30.79 | 80.32 | 62.85 | | | 74.02 | 89.31 | 83.82 | | |
| | | Overall | 94.35 | 81.46 | 87.67 | | | 95.38 | 81.99 | 88.43 | | | 88.82 | 84.19 | 86.42 | | |
| | 64 | NF vs WC-PPG | 85.49 | 97.99 | 86.37 | 35.4 | 3087169 | 98.51 | 95.60 | 98.30 | 35.7 | 3112129 | 97.55 | 95.42 | 97.40 | 37.8 | 3137089 |
| | | NF vs SYN-RN-PPG | 87.20 | 99.99 | 97.33 | | | 99.09 | 100.00 | 99.60 | | | 96.80 | 100.00 | 99.33 | | |
| | | NF vs SYN-ACCE-PPG | 69.89 | 94.27 | 85.51 | | | 71.72 | 82.67 | 78.73 | | | 48.33 | 84.87 | 71.75 | | |
| | | Overall | 82.24 | 91.44 | 87.01 | | | 95.55 | 81.67 | 88.35 | | | 93.89 | 87.54 | 90.60 | | |

**TABLE 5. Optimal parameters for the CNN-based raw and derivative PPG-SQA methods.**

| Method | Optimal Parameters | Noise-Free vs WC-PPG | | | Noise-Free vs SYN-RN-PPG | | | Noise-Free vs SYN-ACCE-PPG | | |
|---|---|---|---|---|---|---|---|---|---|---|
| | | SE (%) | SP (%) | ACC (%) | SE (%) | SP (%) | ACC (%) | SE (%) | SP (%) | ACC (%) |
| Raw PPG [59] | 4 (CLs), 32 (F), ReLU (AF), 6.52 (MS(MB)), 532449 (NP) | 99.96 | 94.84 | 99.58 | 99.96 | 100.00 | 99.99 | 99.99 | 69.76 | 75.80 |
| Proposed (dPPG-1D-CNN-SQA) | 6 (CLs), 32 (F), ReLU (AF), 18.9 (MS(MB)), 1552097 (NP) | 99.84 | 97.94 | 99.70 | 99.79 | 100.00 | 99.96 | 84.48 | 74.63 | 78.17 |

model memory size and improve the convergence speed of the method. Table 6 shows the results of computational complexity analysis in terms of classification accuracy, non-linear activation functions (ReLU, LeakyReLU, and Tanh), kernels (16, 32, and 64), layers (2, 4, and 6) and processing time (PT) for dPPG-based 1D-CNN-SQA methods using different acceptable and unacceptable derivative PPG segments. Results showed that PT (ms) increases when the same

**TABLE 6. Computational complexity of 2, 4, 6-layer dPPG-based 1D-CNN-SQA methods in terms of accuracy, processing time, different activation functions, and number of filters for clean versus noisy segments from various databases.**

| Activation Function | Number of filters | NF versus Noisy PPG signal | Performance of 2-Layer | | | Performance of 4-Layer | | | Performance of 6-Layer | | |
|---|---|---|---|---|---|---|---|---|---|---|---|
| | | | ACC (%) | PT(ms) | | ACC (%) | PT(ms) | | ACC (%) | PT(ms) | |
| | | | | PC-CPU | R-Pi | | PC-CPU | R-Pi | | PC-CPU | R-Pi |
| | | NF vs WC-PPG | 99.17 | 44.3±11.6 | 256.2±53.5 | 94.42 | 47.6±14.1 | 254.9±65.0 | 98.49 | 46.0±19.5 | 251.2±87.2 |
| | 16 | NF vs SYN-RN-PPG | 99.96 | 45.7±8.6 | 254.6±71.4 | 98.81 | 45.1±13.5 | 244.4±47.0 | 99.67 | 48.6±23.6 | 246.3±52.6 |
| | | NF vs SYN-ACCE-PPG | 72.39 | 44.0±11.2 | 253.2±71.4 | 74.02 | 45.7±10.9 | 251.6±48.6 | 73.65 | 47.8±16.3 | 247.3±75.4 |
| | | **NF vs MA-DB01** | 98.87 | 44.2±7.2 | 243.0±41.1 | 98.65 | 46.7±10.9 | 252.9±68.4 | **99.70** | **51.5±16.7** | **255.8±103.6** |
| **ReLU** | **32** | **NF vs SYN-RN-PPG** | 99.54 | 44.2±7.7 | 244.2±54.0 | 99.75 | 48.4±13.7 | 253.4±58.6 | **99.96** | **47.1±12.4** | **249.4±60.6** |
| | | **NF vs SYN-ACCE-PPG** | 62.32 | 44.3±11.7 | 244.1±33.4 | 78.66 | 47.0±11.1 | 257.4±66.1 | **78.17** | **48.6±13.5** | **248.2±62.5** |
| | | NF vs MA-DB01 | 98.18 | 45.1±7.1 | 244.4±37.2 | 90.39 | 49.1±10.9 | 250.3±38.6 | 98.53 | 51.6±16.6 | 253.6±53.4 |
| | 64 | NF vs SYN-RN-PPG | 99.70 | 47.9±8.6 | 247.0±53.9 | 97.73 | 51.1±14.2 | 342.5±15.5 | 99.75 | 52.1±16.2 | 355.0±134.6 |
| | | NF vs SYN-ACCE-PPG | 69.43 | 47.6±12.4 | 255.5±43.6 | 76.10 | 48.7±11.1 | 292.6±115.1 | 61.99 | 52.7±13.3 | 275.3±82.6 |
| | | NF vs MA-DB01 | 97.45 | 43.4±10.6 | 256.2±60.8 | 89.80 | 44.6±12.8 | 246.2±467 | 95.07 | 49.0±12.2 | 248.9±67.4 |
| | 16 | NF vs SYN-RN-PPG | 99.49 | 46.1±12.2 | 244.8±54.4 | 98.25 | 44.3±8.2 | 252.0±52.8 | 99.14 | 46.6±13.3 | 248.5±57.5 |
| | | NF vs SYN-ACCE-PPG | 79.84 | 45.6±11.6 | 250.0±47.0 | 85.89 | 50.4±16.0 | 255.9±63.5 | 88.92 | 44.8±12.8 | 243.1±43.5 |
| | | NF vs MA-DB01 | 95.12 | 47.6±12.6 | 241.6±37.9 | 87.65 | 47.8±12.2 | 251.0±59.3 | 96.40 | 48.3±1.5 | 255.1±68.3 |
| LeakyReLU | 32 | NF vs SYN-RN-PPG | 99.12 | 43.7±10.8 | 239.4±37.9 | 97.79 | 48.5±12.9 | 251.7±59.2 | 99.38 | 46.5±14.8 | 244.6±66.0 |
| | | NF vs SYN-ACCE-PPG | 84.39 | 43.5±10.3 | 245.8±37.1 | 93.20 | 46.1±13.4 | 254.8±54.4 | 80.10 | 48.1±13.4 | 256.0±74.2 |
| | | NF vs MA-DB01 | 91.72 | 45.0±10.0 | 314.3±122.4 | 90.99 | 48.3±16.4 | 355.2±138.7 | 99.30 | 48.7±13.0 | 395.7±149.3 |
| | 64 | NF vs SYN-RN-PPG | 98.48 | 48.6±13.2 | 272.9±89.1 | 98.46 | 53.4±13.5 | 386.3±182.1 | 99.91 | 51.1±13.3 | 303.4±137.1 |
| | | NF vs SYN-ACCE-PPG | 87.29 | 48.7±11.7 | 254.0±46.1 | 86.39 | 49.2±9.3 | 258.4±68.8 | 71.74 | 54.4±13.1 | 270.4±89.5 |
| | | NF vs MA-DB01 | 98.79 | 43.6±11.3 | 239.6±35.7 | 97.73 | 44.4±11.2 | 250.5±67.5 | 97.06 | 50.5±15.5 | 244.9±76.7 |
| | 16 | NF vs SYN-RN-PPG | 99.72 | 46.0±12.5 | 238.9±41.1 | 99.46 | 44.3±11.2 | 252.0±55.3 | 99.41 | 46.2±14.7 | 245.6±73.6 |
| | | NF vs SYN-ACCE-PPG | 79.80 | 45.6±8.2 | 247.2±49.5 | 68.80 | 53.0±16.3 | 244.5±52.3 | 83.72 | 47.5±13.5 | 250.1±51.2 |
| | | NF vs MA-DB01 | 96.56 | 47.2±12.0 | 247.0±53.3 | 98.35 | 49.6±13.4 | 254.8±54.8 | 95.80 | 48.2±12.2 | 250.9±73.1 |
| Tanh | 32 | NF vs SYN-RN-PPG | 99.35 | 43.1±9.3 | 255.5±214.5 | 99.57 | 45.2±8.9 | 249.6±44.3 | 99.08 | 47.2±14.1 | 250.5±54.8 |
| | | NF vs SYN-ACCE-PPG | 75.78 | 43.3±5.4 | 247.8±33.9 | 62.85 | 50.0±13.0 | 252.0±55.8 | 83.82 | 47.6±14.7 | 250.2±55.9 |
| | | NF vs MA-DB01 | 86.37 | 44.9±9.7 | 257.8±73.1 | 98.30 | 51.5±12.9 | 337.0±147.6 | 97.40 | 50.1±10.2 | 312.1±120.2 |
| | 64 | NF vs SYN-RN-PPG | 97.33 | 49.2±11.6 | 342.3±161.9 | 99.60 | 53.2±10.0 | 340.1±152.3 | 99.33 | 47.4±12.6 | 305.6±141.1 |
| | | NF vs SYN-ACCE-PPG | 85.51 | 46.0±6.0 | 254.8±51.3 | 78.73 | 50.4±13.5 | 275.8±84.0 | 71.75 | 53.5±14.5 | 256.5±54.1 |

**TABLE 7. Performance comparison of 6-layer dPPG-based 1D-CNN-SQA method with other non-DL methods.**

| Method | Model Size | Performance | | |
|---|---|---|---|---|
| | (kB) | SE (%) | SP (%) | ACC (%) |
| [14] | 29.56 | 98.22 | 90.71 | 93.21 |
| SVM (RBF) [14] | 126.85 | 98.22 | 88.59 | 91.80 |
| SVM (Linear) [14] | 141.7 | 98.39 | 87.85 | 91.36 |
| [16] | NR | 99.29 | 95.31 | 97.76 |
| SVM [47] | NR | 93.25 | 91.90 | NR |
| [48] | NR | 91.00 | 95.00 | NR |
| SE [49] | NR | 85.00 | 99.40 | 87.40 |
| Kurtosis [49] | NR | 72.60 | 98.60 | 77.00 |
| SE+Kurtosis [49] | NR | 86.90 | 98.30 | 88.80 |
| dPPG-1D-CNN-SQA | 18900 | 99.79 | 100.00 | 99.96 |

1D-CNN model is implemented on the R-Pi (model B, having the Quad-Core Cortex-A72 processor and 8 GB LPDDR4 RAM) compared to PC-CPU platform (Intel Xeon (R) E52620 CPU running at 2.40 GHz, with 40 GB RAM), see Table 6.

### *B. REAL-TIME VALIDATION USING R-PI COMPUTING PLATFORM*

In recent years, PPG technology-embedded wearable and portable healthcare devices have gained more popularity due to their noninvasive, simple, and cost-effective nature.

**TABLE 8. Comparison of the existing 1D-CNN-based PPG-SQA methods with the proposed 6-layer dPPG-based 1D-CNN-SQA model in terms of performance metrics.**

| Method | Model | No. of Layers | Activation Function | No. of Filters | Performance | | |
|---|---|---|---|---|---|---|---|
| | | | | | SE (%) | SP (%) | ACC (%) |
| [1] | 1D-CNN | NR | ReLU | 196 | 83.33 | 83.54 | NR |
| [17] | 1D-CNN | 13 CLs | ReLU | 50 | NR | NR | 94.50 |
| [57] | 1D-CNN | 3 CLs | ReLU | 8 | NR | NR | 90.02 |
| [58] | 1D-CNN | 4 CLs | ReLU | 32 | NR | NR | 86 and 81 |
| [59]* | 1D-CNN | 4 CLs | ReLU | 32 | 99.96 | 100.00 | 99.99 |
| dPPG-1D-CNN-SQA | 1D-CNN | 6 CLs | ReLU | 32 | 99.79 | 100.00 | 99.96 |

However, these PPG healthcare devices are limited in terms of battery capacity, onboard memory, and processor speed [3], [76]. Therefore, it is important to verify the real-time feasibility of the method before deploying it on resource-constrained PPG analysis devices. In this work, the real-time feasibility of the 1D-CNN models was tested using R-Pi computing platform. Fig. 5a shows the real-time validation of the dPPG-based optimal 1D-CNN-SQA model by using the R-Pi computing platform and standard untrained datasets and its implementation steps are summarized below:

- Essential back-end (Tensor Flow) and frond-end (Keras) deep learning libraries are installed using the package manager for Python (PIP).
- To evaluate the proposed method in the Jupyter Notebook platform, several important libraries are imported: Matplotlib, Pandas, Numpy, and Sklearn.
- To perform the derivative PPG signal classification, the test clean and noisy databases (.csv files) are read using "*pd.read command*".
- The trained 1D-CNN models are loaded into R-Pi using "*keras.models.load command*", see Fig. 3(c).
- Finally, clean and noisy derivative classes are predicted using the "*model.predict command*".

### C. PERFORMANCE COMPARISON

Table 7 summarizes the performance comparison of non-DL PPG-SQA methods with the proposed 6-layer dPPG-based 1D-CNN-SQA method in terms of evaluation metrics and model capacity (kB). Our dPPG-based 1D-CNN-SQA model with 6 layers performs better and requires less memory, as shown in Table 7. However, the memory size of the many methods is not reported, which is important for deployment of the model in a real-time computing platform, see Table 7. Similarly, Table 8 summarizes the performance comparison of existing 1D-CNN-based PPG-SQA methods with the proposed 6-layer dPPG-based 1D-CNN-SQA method in terms of model capacity (kB), number of CLs, AFs, and number of kernels. Comparison results demonstrate that the 6-layer dPPG-based 1D-CNN-SQA model outperforms the existing non-DL and DL PPG-SQA

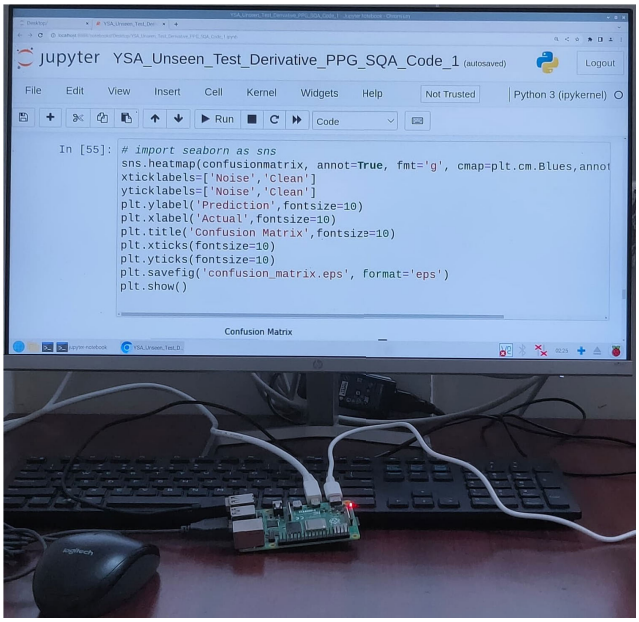


(a) The overall R-Pi block diagram of the 1D-CNN-based derivative PPG-SQA method.

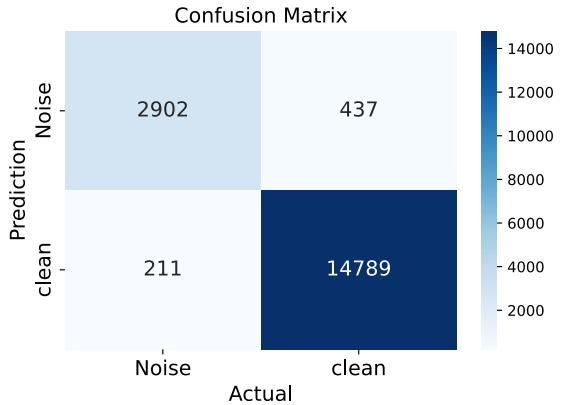


(b) Confusion matrix of the 1D-CNN-based derivative PPG-SQA method.

**FIGURE 5. Illustrates real-time implementation of the optimal derivative model (6-layer and 32 kernels with ReLU activation function) and performance evaluation using an untrained database (UCI). (a) Loaded the untrained database test jupyter notebook python code in the R-Pi platform, and (b) evaluated the confusion matrix of the UCI unseen database.**

**TABLE 9.** Performance evaluation of the unseen databases using 6-layer dPPG-based 1D-CNN-SQA model.

| Database | Total Segments | TN | FP | FN | TP | Performance | | |
|---|---|---|---|---|---|---|---|---|
| | | | | | | SE (%) | SP(%) | ACC(%) |
| UCI [73] | 18339 | 2902 | 437 | 211 | 14789 | 98.59 | 86.91 | 96.47 |
| VitaDB [74] | 8796 | 1613 | 245 | 388 | 6550 | 94.41 | 86.81 | 92.80 |
| PulseDB [75] | 31920 | 1542 | 378 | 771 | 29229 | 97.43 | 80.31 | 96.40 |

methods, see Table 8. Further, our dPPG-based 1D-CNN model (6-layer with 32 and ReLU AF) was evaluated with three unseen databases such as UCI, VitalDB, and PulseDB, see Table 9. It is to be noted that the aforementioned databases were used to estimate the blood pressure [73], [74], [75], and our dPPG-based 1D-CNN method gave better signal quality assessment for these databases, showing the efficacy of the dPPG-based 1D-CNN-SQA method. Since, many studies demonstrated that the quality of the signal improves the vital sign parameter extraction and disease classification [57], [58]. Therefore, our optimal 1D-CNN-based derivative model can be used for the automatic quality assessment stage in blood pressure estimation methods to achieve better performance.

## VI. CONCLUSION

The raw and derivative PPG-SQA are essential to accurately estimating vital sign parameters such as pulse rate, pulse rate variability, respiration rate, blood pressure, and blood glucose level in healthcare devices. Therefore, in this work, we developed a dPPG-based 1D-CNN-SQA method using different convolution layers (2, 4, and 6), activation functions (ReLU, LeakyReLU, and Tanh), and kernels (16, 32, and 64 with a size of 3). The clean and noisy PPG segments were considered from different standard databases and pre-processed using different signal-processing techniques. The pre-processed derivative PPG signals were fed as input to 2, 4, and 6-layer 1D-CNN models (a total of 27 models) to identify the best-fit model that classifies the PPG signals as clean or noisy. A total of 27 models were evaluated using a known database, the best-fit (6-layer with 32 kernels and ReLU activation function) model achieved an accuracy of 99.70% (average PT (ms) of 51.5 $\pm$ 16.7) for NF versus WC-PPG, 99.96% (average PT (ms) of 47.1$\pm$12.4) for NF versus SYN-RN-PPG, 78.17% (average PT (ms) of 48.6$\pm$13.5) for NF versus SYN-ACCE-PPG, and 88.82% for overall database. The method was also implemented using the Raspberry Pi module to verify the real-time feasibility, where it achieved an average PT (ms) of 255.8$\pm$103.6 for NF vs WC-PPG, 249.4$\pm$60.6 for NF vs SYN-RN-PPG, and 248.2$\pm$62.5 for NF vs SYN-ACCE-PPG databases. The dPPG-based 1D-CNN-SQA method, with the best optimal parameters, has great potential for reducing false alarms and the overall energy consumption of health and wellness monitoring devices with limited computational resources and battery capacity.

## REFERENCES

[1] E. K. Naeini, I. Azimi, A. M. Rahmani, P. Liljeberg, and N. Dutt, "A real-time PPG quality assessment approach for healthcare Internet-of-Things," *Proc. Comput. Sci.*, vol. 151, pp. 551–558, Jan. 2019.
[2] U. Satija, B. Ramkumar, and M. S. Manikandan, "Real-time signal quality-aware ECG telemetry system for IoT-based health care monitoring," *IEEE Internet Things J.*, vol. 4, no. 3, pp. 815–823, Jun. 2017.
[3] P. N. Sivaranjini, M. S. Manikandan, and L. R. Cenkeramaddi, "Lightweight photoplethysmogram waveform change detection for resource-constrained IoT enabled remote health monitoring devices," in *Proc. 11th Int. Conf. Control, Mechatronics Autom. (ICCMA)*, Nov. 2023, pp. 330–335.
[4] G. N. K. Reddy, M. S. Manikandan, N. V. L. N. Murty, and L. R. Cenkeramaddi, "Unified quality-aware compression and pulse-respiration rates estimation framework for reducing energy consumption and false alarms of wearable PPG monitoring devices," *IEEE Access*, vol. 11, pp. 41708–41740, 2023.
[5] P. N. Sivaranjini, M. S. Manikandan, and L. R. Cenkeramaddi, "Compressed sensing based $SpO_2$ and PR estimation for improving resource utilization efficiency of wearables in IoMT applications," in *Proc. IEEE 9th Int. Conf. Smart Instrum., Meas. Appl. (ICSIMA)*, Oct. 2023, pp. 30–35.
[6] S.-H. Liu, H.-C. Liu, W. Chen, and T.-H. Tan, "Evaluating quality of photoplethymographic signal on wearable forehead pulse oximeter with supervised classification approaches," *IEEE Access*, vol. 8, pp. 185121–185135, 2020.
[7] G. N. K. Reddy, M. S. Manikandan, and N. V. L. N. Murty, "Predictive coding with simultaneous extraction of pulse and respiration rates from PPG signal for energy constrained wearable devices," in *Proc. 4th Int. Conf. Bio-Eng. Smart Technol. (BioSMART)*, Dec. 2021, pp. 1–4.
[8] K. Manojkumar, S. Boppu, and M. S. Manikandan, "An automated algorithm for estimating respiration rate from PPG signals," in *Proc. 2nd Int. Conf. Mach. Learn. Image Process. Netw. Secur. Data Sci. (MIND)*, vol. 1241, Silchar, India. Springer, Jul. 2020, pp. 44–57.
[9] S. Haddad, A. Boukhayma, and A. Caizzone, "Continuous PPG-based blood pressure monitoring using multi-linear regression," *IEEE J. Biomed. Health Informat.*, vol. 26, no. 5, pp. 2096–2105, May 2022.
[10] M. Liu, L.-M. Po, and H. Fu, "Cuffless blood pressure estimation based on photoplethysmography signal and its second derivative," *Int. J. Comput. Theory Eng.*, vol. 9, no. 3, pp. 202–206, 2017.
[11] N. S. Shilpa, V. J. Varghese, P. N. Sivaranjini, A. K. Panda, M. S. Manikandan, and R. B. Pachori, "Performance evaluation of cuffless blood pressure estimation methods using linear and non-linear models with PTT and PR parameters," in *Proc. 9th Int. Conf. Signal Process. Commun. (ICSC)*, Dec. 2023, pp. 397–402.
[12] S. Chen, F. Qin, X. Ma, J. Wei, Y.-T. Zhang, Y. Zhang, and E. Jovanov, "Multi-view cross-fusion transformer based on kinetic features for non-invasive blood glucose measurement using PPG signal," *IEEE J. Biomed. Health Informat.*, vol. 28, no. 4, pp. 1982–1992, Apr. 2024.
[13] J. Chen, K. Sun, Y. Sun, and X. Li, "Signal quality assessment of PPG signals using STFT time-frequency spectra and deep learning approaches," in *Proc. 43rd Annu. Int. Conf. IEEE Eng. Med. Biol. Soc. (EMBC)*, Nov. 2021, pp. 1153–1156.
[14] G. N. K. Reddy, M. S. Manikandan, and N. V. L. N. Murty, "On-device integrated PPG quality assessment and sensor disconnection/saturation detection system for IoT health monitoring," *IEEE Trans. Instrum. Meas.*, vol. 69, no. 9, pp. 6351–6361, Sep. 2020.
[15] G. N. K. Reddy, M. S. Manikandan, and N. V. L. N. Murty, "Evaluation of objective distortion measures for automatic quality assessment of processed PPG signals for real-time health monitoring devices," *IEEE Access*, vol. 10, pp. 15707–15745, 2022.

[16] S. Vadrevu and M. S. Manikandan, "Real-time PPG signal quality assessment system for improving battery life and false alarms," *IEEE Trans. Circuits Syst. II, Exp. Briefs*, vol. 66, no. 11, pp. 1910–1914, Nov. 2019.

[17] C.-H. Goh, L. K. Tan, N. H. Lovell, S.-C. Ng, M. P. Tan, and E. Lim, "Robust PPG motion artifact detection using a 1-D convolution neural network," *Comput. Methods Programs Biomed.*, vol. 196, Nov. 2020, Art. no. 105596.

[18] K. Q. Yousef, U. Rubins, and A. Mafawez, "Photoplethysmogram second derivative review: Analysis and applications," *Sci. Res. Essays*, vol. 10, no. 21, pp. 633–639, Nov. 2015.

[19] S. Vadrevu and M. S. Manikandan, "A robust pulse onset and peak detection method for automated PPG signal analysis system," *IEEE Trans. Instrum. Meas.*, vol. 68, no. 3, pp. 807–817, Mar. 2019.

[20] S. Vadrevu and M. S. Manikandan, "Effective systolic peak detection algorithm using variational mode decomposition and center of gravity," in *Proc. IEEE Region 10 Conf. (TENCON)*, Nov. 2016, pp. 2711–2715.

[21] S. Gupta, A. Singh, and A. Sharma, "Exploiting moving slope features of PPG derivatives for estimation of mean arterial pressure," *Biomed. Eng. Lett.*, vol. 13, no. 1, pp. 1–9, Feb. 2023.

[22] S. Gupta, A. Singh, and A. Sharma, "Dynamic large artery stiffness index for cuffless blood pressure estimation," *IEEE Sensors Lett.*, vol. 6, no. 3, pp. 1–4, Mar. 2022.

[23] S. Vadrevu and M. S. Manikandan, "Real-time quality-aware PPG waveform delineation and parameter extraction for effective unsupervised and IoT health monitoring systems," *IEEE Sensors J.*, vol. 19, no. 17, pp. 7613–7623, Sep. 2019.

[24] S. Bhowmick, P. K. Kundu, and D. D. Mandal, "Determination of fiducial parameter of PPG signal by second derivative method," in *Proc. Michael Faraday IET Int. Summit (MFIIS)*, Oct. 2020, pp. 52–58.

[25] H. Samimi and H. R. Dajani, "A PPG-based calibration-free cuffless blood pressure estimation method using cardiovascular dynamics," *Sensors*, vol. 23, no. 8, p. 4145, Apr. 2023.

[26] C. El Hajj and P. A. Kyriacou, "Cuffless and continuous blood pressure estimation from PPG signals using recurrent neural networks," in *Proc. 42nd Annu. Int. Conf. IEEE Eng. Med. Biol. Soc. (EMBC)*, Jul. 2020, pp. 4269–4272.

[27] S. Gupta, A. Singh, A. Sharma, and R. K. Tripathy, "Higher order derivative-based integrated model for cuff-less blood pressure estimation and stratification using PPG signals," *IEEE Sensors J.*, vol. 22, no. 22, pp. 22030–22039, Nov. 2022.

[28] L.-H. Wang, K.-K. Sun, C.-X. Xie, M.-H. Fan, P. A. R. Abu, and P.-C. Huang, "Cuffless blood pressure estimation using dual physiological signal and its morphological features," *IEEE Sensors J.*, vol. 23, no. 11, pp. 11956–11967, Jun. 2023.

[29] J. Hong, J. Gao, Q. Liu, Y. Zhang, and Y. Zheng, "Deep learning model with individualized fine-tuning for dynamic and beat-to-beat blood pressure estimation," in *Proc. IEEE 17th Int. Conf. Wearable Implant. Body Sensor Netw. (BSN)*, Jul. 2021, pp. 1–4.

[30] G. N. K. Reddy, M. S. Manikandan, and R. B. Pachori, "Automated Hilbert envelope based respiration rate measurement from PPG signal for wearable vital signs monitoring devices," in *Proc. Int. Conf. Artif. Intell. Things (ICAIoT)*, Dec. 2022, pp. 1–6.

[31] G. N. K. Reddy, M. S. Manikandan, and N. V. L. N. Murty, "Integrated data compression and pulse rate extraction scheme using differential coding for wireless PPG monitoring devices," in *Proc. IEEE 13th Int. Conf. Ind. Inf. Syst. (ICIIS)*, Dec. 2018, pp. 48–53.

[32] T. Choudhary and M. S. Manikandan, "Robust photoplethysmographic (PPG) based biometric authentication for wireless body area networks and m-health applications," in *Proc. 22nd Nat. Conf. Commun. (NCC)*, Mar. 2016, pp. 1–6.

[33] K. K. Pulluri, M. S. Manikandan, P. N. Sivaranjini, and R. B. Pachori, "Performance evaluation of ten $SpO_2$ measurement equations using estimation error range metric and different signal lengths," in *Proc. IEEE 9th Int. Conf. Smart Instrum., Meas. Appl. (ICSIMA)*, Oct. 2023, pp. 18–23.

[34] P. N. Sivaranjini and M. S. Manikandan, "Computationally-efficient pulse rate estimation from compressed PPG measurements for continuous vital signs monitoring," in *Proc. 5th Int. Conf. Bio-Eng. Smart Technol. (BioSMART)*, Jun. 2023, pp. 1–4.

[35] M. N. I. Shuzan, M. H. Chowdhury, M. E. H. Chowdhury, K. Abualsaud, E. Yaacoub, M. A. A. Faisal, M. Alshahwani, N. Al Bordeni, F. Al-Kaabi, S. Al-Mohannadi, S. Mahmud, and N. Zorba, "QU-GM: An IoT based glucose monitoring system from photoplethysmography, blood pressure, and demographic data using machine learning," *IEEE Access*, vol. 12, pp. 77774–77790, 2024.

[36] S. Vadrevu and M. S. Manikandan, "Use of zero-frequency resonator for automatically detecting systolic peaks of photoplethysmogram signal," *Healthcare Technol. Lett.*, vol. 6, no. 3, pp. 53–58, Jun. 2019.

[37] M. Z. Suboh, R. Jaafar, N. A. Nayan, N. H. Harun, and M. S. F. Mohamad, "Analysis on four derivative waveforms of photoplethysmogram (PPG) for fiducial point detection," *Frontiers Public Health*, vol. 10, Jun. 2022, Art. no. 920946.

[38] R. M. Rozi, S. Usman, M. A. M. Ali, and M. B. I. Reaz, "Second derivatives of photoplethysmography (PPG) for estimating vascular aging of atherosclerotic patients," in *Proc. IEEE-EMBS Conf. Biomed. Eng. Sci.*, Dec. 2012, pp. 256–259.

[39] M. Salah, O. A. Omer, L. Hassan, M. Ragab, A. M. Hassan, and A. Abdelreheem, "Beat-based PPG-ABP cleaning technique for blood pressure estimation," *IEEE Access*, vol. 10, pp. 55616–55626, 2022.

[40] T. Chatterjee, A. Ghosh, and S. Sarkar, "Signal quality assessment of photoplethysmogram signals using quantum pattern recognition technique and lightweight CNN module," in *Proc. 44th Annu. Int. Conf. IEEE Eng. Med. Biol. Soc. (EMBC)*, Jul. 2022, pp. 3382–3386.

[41] D. Roh and H. Shin, "Recurrence plot and machine learning for signal quality assessment of photoplethysmogram in mobile environment," *Sensors*, vol. 21, no. 6, p. 2188, Mar. 2021.

[42] S. Vadrevu and M. S. Manikandan, "A new quality-aware quality-control data compression framework for power reduction in IoT and smartphone PPG monitoring devices," *IEEE Sensors Lett.*, vol. 3, no. 7, pp. 1–4, Jul. 2019.

[43] G. N. K. Reddy, M. S. Manikandan, and N. V. L. N. Murty, "Lightweight compressed sensing (CS) and partial DCT based compression schemes for energy-efficient wearable PPG monitoring devices," in *Proc. IEEE Int. Conf. Health, Instrum. Meas., Natural Sci. (InHeNce)*, Jul. 2021, pp. 1–6.

[44] M. A. Jayarani, M. S. Manikandan, and S. Mula, "Performance evaluation of sparse recovery algorithms for efficient signal reconstruction in compressed PPG sensing node," in *Proc. IEEE 9th Int. Conf. Smart Instrum., Meas. Appl. (ICSIMA)*, Oct. 2023, pp. 36–41.

[45] P. N. Sivaranjini, M. S. Manikandan, and L. R. Cenkeramaddi, "Fast quality-aware AMDF based pulse rate estimation from compressed PPG measurements for wearable vital signs monitor," in *Proc. 15th Int. Conf. Electron., Comput. Artif. Intell. (ECAI)*, Jun. 2023, pp. 01–06.

[46] G. N. K. Reddy, M. S. Manikandan, and N. V. L. N. Murty, "Information theoretic metrics for automatic quality assessment of processed PPG signals," in *Proc. 3rd Int. Conf. Electr. Electron. Eng. (ICEEE)*, Dec. 2021, pp. 157–160.

[47] E. Sabeti, N. Reamaroon, M. Mathis, J. Gryak, M. Sjoding, and K. Najarian, "Signal quality measure for pulsatile physiological signals using morphological features: Applications in reliability measure for pulse oximetry," *Informat. Med. Unlocked*, vol. 16, Jan. 2019, Art. no. 100222.

[48] C. Orphanidou, T. Bonnici, P. Charlton, D. Clifton, D. Vallance, and L. Tarassenko, "Signal-quality indices for the electrocardiogram and photoplethysmogram: Derivation and applications to wireless monitoring," *IEEE J. Biomed. Health Informat.*, vol. 19, no. 3, pp. 832–838, May 2015.

[49] N. Selvaraj, Y. Mendelson, K. H. Shelley, D. G. Silverman, and K. H. Chon, "Statistical approach for the detection of motion/noise artifacts in photoplethysmogram," in *Proc. Annu. Int. Conf. IEEE Eng. Med. Biol. Soc.*, Aug. 2011, pp. 4972–4975.

[50] J. A. Sukor, S. J. Redmond, and N. H. Lovell, "Signal quality measures for pulse oximetry through waveform morphology analysis," *Physiol. Meas.*, vol. 32, no. 3, pp. 369–384, Mar. 2011.

[51] G. B. Papini, P. Fonseca, X. L. Aubert, S. Overeem, J. W. M. Bergmans, and R. Vullings, "Photoplethysmography beat detection and pulse morphology quality assessment for signal reliability estimation," in *Proc. 39th Annu. Int. Conf. IEEE Eng. Med. Biol. Soc. (EMBC)*, Jul. 2017, pp. 117–120.

[52] W. Karlen, K. Kobayashi, J. M. Ansermino, and G. A. Dumont, "Photoplethysmogram signal quality estimation using repeated Gaussian filters and cross-correlation," *Physiol. Meas.*, vol. 33, no. 10, pp. 1617–1629, Oct. 2012.

[53] M. Elgendi, "Optimal signal quality index for photoplethysmogram signals," *Bioengineering*, vol. 3, no. 4, p. 21, Sep. 2016.

[54] S.-H. Liu, R.-X. Li, J.-J. Wang, W. Chen, and C.-H. Su, "Classification of photoplethysmographic signal quality with deep convolution neural networks for accurate measurement of cardiac stroke volume," *Appl. Sci.*, vol. 10, no. 13, p. 4612, Jul. 2020.

[55] T. Pereira, C. Ding, K. Gadhoumi, N. Tran, R. A. Colorado, K. Meisel, and X. Hu, "Deep learning approaches for plethysmography signal quality assessment in the presence of atrial fibrillation," *Physiol. Meas.*, vol. 40, no. 12, Dec. 2019, Art. no. 125002.

[56] F. Esgalhado, B. Fernandes, V. Vassilenko, A. Batista, and S. Russo, "The application of deep learning algorithms for PPG signal processing and classification," *Computers*, vol. 10, no. 12, p. 158, Nov. 2021.

[57] A. Aliamiri and Y. Shen, "Deep learning based atrial fibrillation detection using wearable photoplethysmography sensor," in *Proc. IEEE EMBS Int. Conf. Biomed. Health Informat. (BHI)*, Mar. 2018, pp. 442–445.

[58] S. Zanelli, M. A. El Yacoubi, M. Hallab, and M. Ammi, "Transfer learning of CNN-based signal quality assessment from clinical to non-clinical PPG signals," in *Proc. 43rd Annu. Int. Conf. IEEE Eng. Med. Biol. Soc. (EMBC)*, Nov. 2021, pp. 902–905.

[59] Y. Sivanjaneyulu, M. S. Manikandan, and S. Boppu, "CNN based PPG signal quality assessment using raw PPG signal for energy-efficient PPG analysis devices in Internet of Medical Things," in *Proc. Int. Conf. Artif. Intell. Things (ICAIoT)*, Dec. 2022, pp. 1–6.

[60] Y. Sivanjaneyulu, S. Boppu, and M. S. Manikandan, "Compressive sensing-based automatic PPG signal quality assessment using CNN for energy-constrained medical devices," in *Proc. 15th Int. Conf. Electron., Comput. Artif. Intell. (ECAI)*, Jun. 2023, pp. 1–6.

[61] Z. Khan, M. S. Manikandan, and M. Mahmud, "Photoplethysmography signal quality assessment using neighbour edge restricted horizontal visibility graph and machine learning classifiers," in *Proc. 16th Int. Conf. Electron., Comput. Artif. Intell. (ECAI)*, Jun. 2024, pp. 1–6.

[62] S. P. Surapaneni and M. S. Manikandan, "Graph signal processing based classification of noisy and clean PPG signals using machine learning classifiers for intelligent health monitor," in *Proc. 15th Int. Conf. Electron., Comput. Artif. Intell. (ECAI)*, Jun. 2023, pp. 1–6.

[63] N. Phukan, S. Mohine, A. Mondal, M. S. Manikandan, and R. B. Pachori, "Convolutional neural network-based human activity recognition for edge fitness and context-aware health monitoring devices," *IEEE Sensors J.*, vol. 22, no. 22, pp. 21816–21826, Nov. 2022.

[64] D. Kilichev and W. Kim, "Hyperparameter optimization for 1D-CNN-based network intrusion detection using GA and PSO," *Mathematics*, vol. 11, no. 17, p. 3724, Aug. 2023.

[65] H. Aldawsari, S. Al-Ahmadi, and F. Muhammad, "Optimizing 1D-CNN-based emotion recognition process through channel and feature selection from EEG signals," *Diagnostics*, vol. 13, no. 16, p. 2624, Aug. 2023.

[66] (May 24, 2016). *The MIT-BIH Polysomnographic Database*. [Online]. Available: https://physionet.org/physiobank/database/slpdb/

[67] G. Moody and R. Mark, "A database to support development and evaluation of intelligent intensive care monitoring," in *Proc. Comput. Cardiol.*, Sep. 1996, pp. 657–660.

[68] A. E. W. Johnson, T. J. Pollard, L. Shen, L.-W.-H. Lehman, M. Feng, M. Ghassemi, B. Moody, P. Szolovits, L. Anthony Celi, and R. G. Mark, "MIMIC-III, a freely accessible critical care database," *Sci. Data*, vol. 3, no. 1, pp. 1–9, May 2016.

[69] M. A. F. Pimentel, A. E. W. Johnson, P. H. Charlton, D. Birrenkott, P. J. Watkinson, L. Tarassenko, and D. A. Clifton, "Toward a robust estimation of respiratory rate from pulse oximeters," *IEEE Trans. Biomed. Eng.*, vol. 64, no. 8, pp. 1914–1923, Aug. 2017.

[70] D. Jarchi and A. Casson, "Description of a database containing wrist PPG signals recorded during physical exercise with both accelerometer and gyroscope measures of motion," *Data*, vol. 2, no. 1, p. 1, Dec. 2016.

[71] Z. Zhang, Z. Pi, and B. Liu, "TROIKA: A general framework for heart rate monitoring using wrist-type photoplethysmographic signals during intensive physical exercise," *IEEE Trans. Biomed. Eng.*, vol. 62, no. 2, pp. 522–531, Feb. 2015.

[72] (Apr. 4, 2018). *Complex System Laboratory (CSL Benchmark Dataset) and Capnobase*. [Online]. Available: https://borealisdata.ca/dataverse/capnobase

[73] M. H. K. Mohamad, K. Mohammad, and S. Mahdi, "Cuff-less blood pressure estimation," UCI Mach. Learn. Repository, Rep., 2015, doi: 10.24432/C5B602.

[74] H.-C. Lee and C.-W. Jung, "Vital recorder—A free research tool for automatic recording of high-resolution time-synchronised physiological data from multiple anaesthesia devices," *Sci. Rep.*, vol. 8, no. 1, p. 1527, Jan. 2018.

[75] W. Wang, P. Mohseni, K. L. Kilgore, and L. Najafizadeh, "PulseDB: A large, cleaned dataset based on MIMIC-III and VitalDB for benchmarking cuff-less blood pressure estimation methods," *Frontiers Digit. Health*, vol. 4, Feb. 2023, Art. no. 1090854.

[76] P. Dhilleswararao, S. Boppu, M. S. Manikandan, and L. R. Cenkeramaddi, "Efficient hardware architectures for accelerating deep neural networks: Survey," *IEEE Access*, vol. 10, pp. 131788–131828, 2022.

**YALAGALA SIVANJANEYULU** received the B.Tech. degree in electronics and communication engineering from the Vignan Lara Institute of Technology and Science, Guntur, India, in 2015, and the master's degree in signal processing and communication engineering from Acharya Nagarjuna University, Guntur, India, in 2018. He is currently pursuing the Ph.D. degree in electrical sciences with IIT Bhubaneswar, Bhubaneswar, India. His current research interests include signal processing, machine learning, and deep learning.

**M. SABARIMALAI MANIKANDAN** (Senior Member, IEEE) received the B.E. degree in electronics and communication engineering from Bharathiar University, India, the M.E. degree in microwave and optical engineering from Madurai Kamaraj University, India, and the Ph.D. degree in biosignal processing from IIT Guwahati, Assam, India. He was an Assistant Professor with the School of Electrical Sciences, IIT Bhubaneswar (2013–2021). He was a Chief Engineer with the Advanced Technology Group, Samsung India Electronic Pvt. Ltd., Noida, India (2011–2013). He was an Assistant Professor with the Center for Computational Engineering and Networking (CEN), Amrita University, India (2010–2011) and a Lead Engineer (2009–2010) with the Audio Group, Samsung India Electronic Pvt. Ltd. He was a recipient of the 2012 Outstanding Performance Award and also an Employee of the Month during his tenure at Samsung India Electronic Pvt. Ltd. He received the 2019 CVET Most Cited Article Award at the Biomedical Engineering Society (BME) Conference, Philadelphia, USA, and the 2019 IET Healthcare Technology Letters Premium Award. He serves as an Associate Editor for IEEE Access, *Healthcare Technology Letters*, *IET Generation, Transmission & Distribution*, *PLOS Digital Health*, and *Frontiers in Signal Processing* (Biomedical Signal Processing); and an Academic Editor and a Guest Editor of *Journal of Healthcare Engineering*. He serves as a Reviewer for reputed journals including, the IEEE, ACM, IET, Springer, Elsevier, *PLOS One*, and Taylor and Francis. His research interests include the design and development of energy-efficient AI-powered health sensing and monitoring systems, drone detection and see-through wall human sensing, human–machine interactions and voice-enabled technologies, and sound-based surveillance systems. He has published 42 journal articles (in IEEE, Springer, Elsevier, and ACM) and more than 60 conference papers. He has patents in the applications of audio processing and health monitoring: (one U.S. patent granted) and five filed patents (India). He has delivered more than 50 technical talks in both national and international workshops and conferences. He is the Chair of CardioRespiratory (CR) Subgroup of IEEE Standards P1752.2 and a member of working group of IEEE P1924.1 with main contribution of "Recommendation of Sensor and Data Acquisition Techniques."

**SRINIVAS BOPPU** (Member, IEEE) received the joint M.Sc. degree in IC design from Nanyang Technological University (NTU), Singapore, and Technical University of Munich (TUM), Germany, and the Ph.D. degree from the Chair for Hardware/Software Co-Design, Department of Computer Science, University of Erlangen–Nuremberg, Germany, in 2015. He has been an Assistant Professor with the School of Electrical Sciences, IIT Bhubaneswar, since October 2017. Before moving to India, he was a Senior Consultant with Infineon Technologies, Munich, Germany. He was also with Freescale Semiconductors India and ST Microelectronics as a Physical Design Engineer before pursuing the Ph.D. degree. His research interests include high-level synthesis, programmable hardware accelerators, compilers, scheduling and mapping approaches, low power VLSI design, SoC design, and design automation of integrated circuits. He has more than 15 years of experience in both academia and industry in the field of the VLSI domain. He was awarded a full scholarship by Infineon Technologies Asia–Pacific Pte. Ltd., for the M.Sc. degree (IC Design) jointly offered by NTU and TUM.

**LINGA REDDY CENKERAMADDI** (Senior Member, IEEE) received the master's degree in electrical engineering from Indian Institute of Technology Delhi (IIT Delhi), New Delhi, India, in 2004, and the Ph.D. degree in electrical engineering from the Norwegian University of Science and Technology (NTNU), Trondheim, Norway, in 2011. He was with Texas Instruments on mixed signal circuit design before joining the Ph.D. program with NTNU. After finishing the Ph.D. degree, he worked on radiation imaging for an atmosphere space interaction monitor (ASIM Mission to the International Space Station) with the University of Bergen, Bergen, Norway, from 2010 to 2012. He is currently the Leader of the Autonomous and Cyber-Physical Systems (ACPS) Research Group and a Professor with the University of Agder, Grimstad, Norway. He is also a Principal Investigator and a Co-Principal Investigator of many research grants from the Norwegian Research Council. He is also quite active in medical imaging. His research interests include the Internet of Things (IoT), cyber-physical systems, autonomous systems, robotics and automation involving advanced sensor systems, computer vision, thermal imaging, LiDAR imaging, radar imaging, wireless sensor networks, smart electronic systems, advanced machine learning techniques, and connected autonomous systems, including drones/unmanned aerial vehicles (UAVs), unmanned ground vehicles (UGVs), unmanned underwater systems (UUSs), 5G- (and beyond) enabled autonomous vehicles, and socio-technical systems, such as urban transportation systems, smart agriculture, and smart cities. He has co-authored more than 230 research publications that have been published in prestigious international journals and standard conferences in the above research areas. He is a member of ACM. Several of his master's students received the Best Master's Thesis Award in Information and Communication Technology (ICT). He serves as a reviewer for several reputed international conferences and IEEE journals. He is a member of the editorial boards of various international journals and technical program committees of several IEEE conferences.